

Jence Mulder

Lattice matched epitaxial shell growth on InZnP quantum dots

Towards a fully passivated surface



Lattice matched epitaxial shell growth on InZnP quantum dots

Towards a fully passivated surface

By

Jence Theodorus Mulder

in partial fulfilment of the requirements for the degree of

Master of Science
in Chemical Engineering

at the Delft University of Technology,
to be defended publicly on March 8th, 2018 at 09:30 AM.

Supervisor: Dr. A.J. Houtepen
Daily supervisor: Dr. N.R.M. Kirkwood

Thesis committee:	Prof. Dr. F.M. Mulder	TU Delft
	Dr. A.J. Houtepen	TU Delft
	Dr. M. de Puit	TU Delft

An electronic version of this thesis is available at <http://repository.tudelft.nl/>.

Preface

It has been a great opportunity for me to do my master thesis project at the Opto-electronic materials research group in the department of Chemical Engineering of the faculty of Applied sciences from the Delft University of Technology. In the accomplishment of the degree of Master of Science in the area of Chemical Engineering, I am submitting this thesis on “Lattice matched epitaxial shell growth on InZnP quantum dots”.

The whole thesis has been divided into 10 chapters.

- 1 – Introduction
- 2 – Theory
- 3 – Experimental work
- 4 – InZnP core synthesis methods
- 5 – InZnP/ZnMgSe core – shell synthesis
- 6 – ZnMgSe nanoparticle synthesis
- 7 – ZnMgSe synthesis using organometallics
- 8 – InZnP/ZnMgSe synthesis using organometallics
- 9 – InZnP/ZnMgSe/ZnS core – shell – shell synthesis
- 10 – Conclusions

Not only have I been able to finish a very important part of my studies, I also learned a lot more than I expected in advance. This research group and the knowledge and skills of the researchers greatly increased my enthusiasm and interest in this particular field. Therefore, I first of all want to thank Nick Kirkwood for all the help, scientific input, energy and time. Without your supervision, I would have never gotten this far. Good supervision and input have been proven to be much more important than an easily working project.

Secondly, I want to thank Arjan Houtepen for giving me the opportunity to do my project in his research group, but especially for all the opportunities I got offered during my thesis project. Your enthusiasm triggered me to strive for the best results.

Also, I would like to thank the rest of the scientific staff for all the input I got after presentations and meetings and for all the work on the lab that is most often ignored or un(der)appreciated. Without clean and regenerated gloveboxes, there would be no research at all.

At last, I want to thank the bachelor and master students for the great environment in the room. Without the jokes, laughter, music and occasional “singing”, my time would not have been half as good.

*Jence Mulder
Delft, March 2018*

Contents

Abstract.....	i
1. Introduction	1
1.1. Practical applications of quantum dots.....	1
1.2. Problem statement.....	2
2. Theory.....	3
2.1. Electronic band structures of materials	3
2.2. From bulk properties to quantum confinement effects	3
2.3. Energy states in quantum dots.....	4
2.4. Electron excitation and photon emission of quantum dots	6
2.5. The origin of structural defects.....	8
2.6. Possible solutions for removing trap states.....	8
2.7. Thermodynamics of quantum dot synthesis.....	11
2.8. InP quantum dot synthesis.....	13
2.9. Positive effects of Zn.....	14
2.10. Shell growth around InZnP quantum dots.....	14
2.11. Reasoning and aim of the thesis.....	15
3. Experimental work	17
3.1. Used chemicals.....	17
3.2. Used equipment.....	17
3.3. Hot injection synthesis of InZnP core QDs.....	18
3.4. Heating-up synthesis of InZnP core QDs.....	18
3.5. InZnP/Zn(Mg)Se/ZnS synthesis (stearate precursors).....	18
3.6. Zn(Mg)Se synthesis (stearate precursors).....	19
3.7. Zn(Mg)Se synthesis (organometallic precursors).....	20
3.8. InZnP/Zn(Mg)Se/ZnS synthesis (organometallic precursors)	20
4. InZnP core synthesis methods.....	21
4.1. Hot injection method	21
4.2. Heating up method.....	23
4.3. Comparison of the two methods	24
5. InZnP/ZnMgSe core – shell synthesis.....	25
5.1. Necessity of washing cores prior to shell synthesis	25
5.2. The effects of a protective, passivating shell	26
5.3. Lattice matching with ZnMgSe	27
5.4. Shell study required	28
6. ZnMgSe nanoparticle synthesis.....	29
6.1. ZnMgSe synthesis with metal stearates and TBP-Se	29

6.2. More reactive precursors	30
7. ZnMgSe synthesis using organometallics.....	31
7.1. Combined metal precursor synthesis.....	31
7.2. MgSe synthesis for crystallography	32
7.3. ZnS protected ZnMgSe synthesis	33
7.4. Chosen shell growth methods.....	34
8. InZnP/ZnMgSe synthesis using organometallics	35
9. InZnP/ZnMgSe/ZnS core – shell – shell synthesis.....	36
9.1. ZnS shell synthesis on InZnP/ZnMgSe QDs	36
9.2. The beneficial effects of ZnMgSe over ZnSe	37
10. Conclusions	40
10.1. Future research.....	40
Bibliography	- 1 -
Appendix.....	- 4 -
A.1. Derivation for the approximation of a particle in a one dimensional box with infinite potential wells, using the time-independent Schrödinger equation	- 4 -
A.2. Derivation for the approximation of a particle in a three dimensional box with infinite potential wells, using the time-independent Schrödinger equation	- 5 -
A.3. Derivation for the change in free energy for the formation of clusters from monomers.....	- 5 -
A.4. ZnMgSe synthesis with metal stearates and TOP-Se	- 6 -
A.5. Gallium cation exchange on cores.....	- 7 -
A.6. TEM and EDX data section 7.3.	- 9 -

Abstract

Quantum dots are semiconductor nanocrystals that exhibit size specific photophysical properties. Therefore, they can be applied as phosphors in LED lighting and television screens. The main issue regarding currently used quantum dots is that most of them are cadmium based (e.g. cadmium selenide). Because cadmium is highly toxic and carcinogenic, its use is restricted from most commercial applications.

As solution to this problem is an indium based quantum dot, which is far less toxic. The main problem with indium based quantum dots, is a lower photoluminescence quantum yield, a lower stability and a lower color purity. For this reason, in this thesis we aimed to improve the photoluminescence quantum yield by a better quantum dot surface passivation, to reduce the number of non-emitting recombination sites (dangling bonds). To passivate the surface, zinc magnesium selenide was chosen as a shell material that has an improved lattice match compared to currently used materials (such as zinc sulfide and zinc selenide). Furthermore, this zinc magnesium selenide shell should protect the quantum dot from the outside, therefore increasing its stability to air and moisture. Also, the bandgap energy of this material is higher compared to currently used shell materials, so the electron and hole are more confined in the quantum dot core. This automatically should improve the color purity.

The research performed showed that the synthesis of zinc magnesium selenide is quite difficult and cannot be approached the same way as a zinc selenide shell is usually synthesized. Therefore, a method using organometallic precursors was developed to synthesize this material. Results showed that zinc magnesium selenide as a shell material has an improved effect on the photoluminescence quantum yield, stability and color purity of indium phosphide quantum dots, compared to a zinc selenide shell. The synthetic method needs to be optimized before the indium phosphide quantum dots with a zinc magnesium selenide shell are able to compete with cadmium selenide quantum dots.

1. Introduction

Quantum dots (QDs) are nanocrystals of semiconductor materials that, due to their size, exhibit specific photophysical properties that do not occur in their bulk materials. These properties include bright fluorescence and size-dependent absorption and emission bands. [1] These properties arise due to the fact that the quantum dots are much smaller than the exciton Bohr radius, leading to quantum confinement effects (section 2.2.). [2]

1.1. Practical applications of quantum dots

The specific properties of quantum dots are attractive for many fields of academic research, as well as for industry. Research on QDs spans areas such as theoretical studies on photophysical properties of various QD materials. [3-5] Furthermore, QDs are also applicable as phosphors [6, 7], single photon emitters [8, 9], electroluminescent materials [10, 11] and as *in-vivo* tracers for biological research, as they are not biologically degradable, small in size and easily chemically bound to *e.g.* proteins. [12-14]

Several major players in the commercial electronics industry, like Apple Inc. [15, 16], Samsung [17] and SONY [18] are currently also incorporating quantum dots in their newest products. The most well-known example is the QLED television, which has been on the market since 2013. [19] Furthermore, QLED lighting is currently on the market, which has a 5 to 15% better efficiency than previously used phosphors (figure 1.). [20]



Figure 1. Different commercial products that have quantum dots as a main component. A Samsung QE65Q7F QLED tv [21] and a QLED light bulb. [22]

For QLED televisions, the color of the depicted image can be made much more realistic with quantum dots than with currently used phosphors (figure 2a, 2b.). The reason behind this is the improved color purity than previously used phosphors (figure 2c.). Therefore, the amount of different colors a human can observe is greatly increased (figure 3.). In the search for better phosphors, fluorescent organic dyes have also been studied and used, however the organic dyes are less stable and therefore the quality of such a screen will become less after subsequent use. [23, 24]

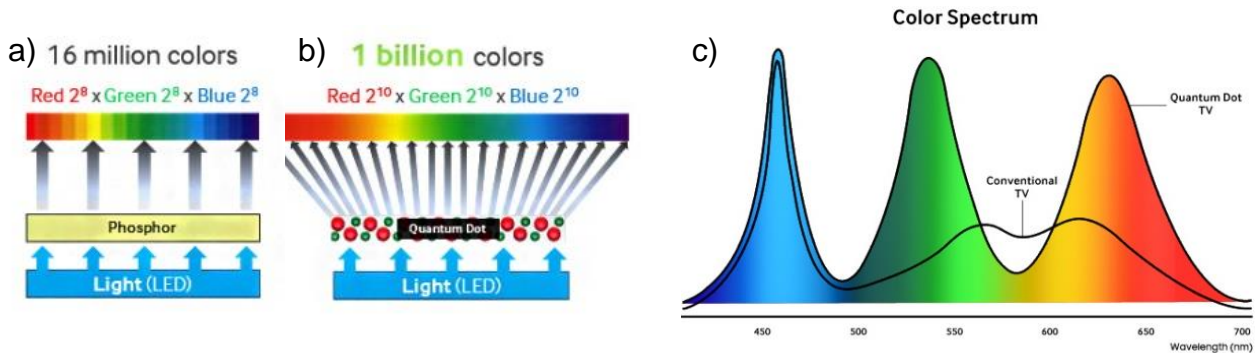


Figure 2. The difference between the number of color tones by using phosphors (a) or quantum dots (b), according to Samsung. The purity of the green and red color is much higher for the quantum dot TV (c). Adjusted from. [25]

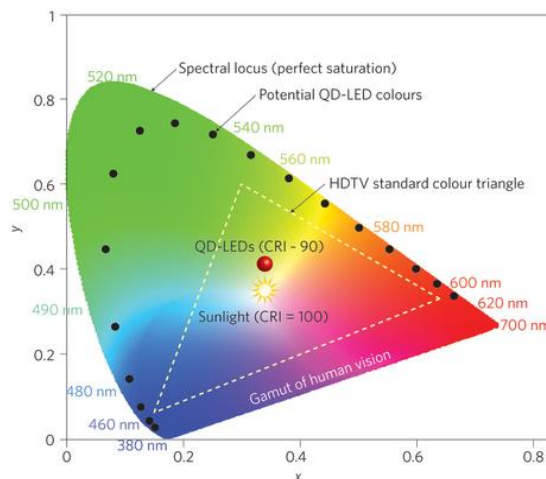


Figure 3. A color triangle, indicating the different colors that can be made by a single pixel, by combining blue, a green and a red light. The white dashed line indicated the limitations of current HDTV's. Quantum dot based phosphors can greatly increase the number of observable colors. [26]

1.2. Problem statement

The main issue with most of the currently used phosphors is that the most studied and thus optimized quantum dots (in terms of photoluminescence quantum yield (PLQY), stability and color purity) are cadmium based quantum dots like cadmium selenide. Cadmium is highly toxic and carcinogenic, and therefore restricted for use in commercial applications. [27] A less toxic alternative for cadmium selenide quantum dots are indium phosphide quantum dots. [28] However, the PLQY, stability and color purity are far less optimized for indium phosphide than for cadmium selenide.

2. Theory

In this chapter, some of the theory relating to relevant properties of QDs for phosphor applications is explained. From this theory, the approaches that were taken during the syntheses to improve the quantum dots can be understood.

2.1. Electronic band structures of materials

In general, all materials can be classified by electrical conductivity as either a conductor (e.g. metals), a semiconductor (e.g. monocrystalline silicon) or an insulator (e.g. sulfur). Semiconductors are materials that have an electrical conductivity between that of conductors and insulators. This is caused by non-overlapping conduction and valence bands that are relatively close together, as can be seen for bulk material in figure 4. The bandgap energy of bulk semiconductors, the energy difference between the conduction and valence band, usually lies between 1 and 3 eV.

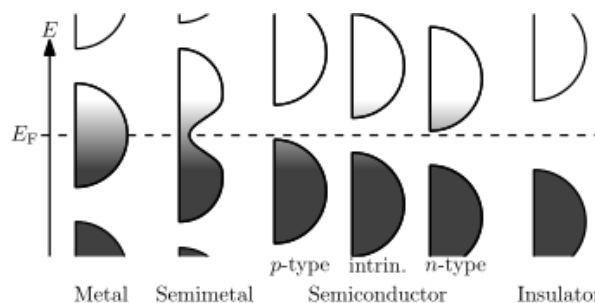


Figure 4. Different materials, classified by electrical conductivity. [29]

2.2. From bulk properties to quantum confinement effects

The energy bands, the conduction and valence band, can be considered to arise from the linear combination of atomic orbitals. By binding two atoms, the atomic orbitals can be added together to give bonding or anti-bonding orbitals, as can be seen in figure 5. When increasing the number of atoms in a single piece of material, the number of possible combinations of bonding and anti-bonding orbitals increases rapidly, leading to two sets of discrete energy levels. For bulk material, the large number of discrete energy levels form energy bands. But when the number of atoms in a crystal is small, the discrete energy levels do not form energy bands. In this region, the material properties are very different from their bulk material. When decreasing the size of a small crystal, the band gap energy increases rapidly as can be seen from figure 5. This leads to the quantum confinement effect, which is clearly visible in nanomaterials such as quantum dots.

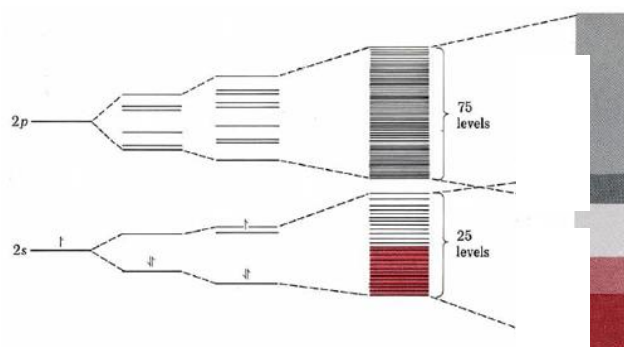


Figure 5. Band splitting for (metal) crystals of different sizes. Small crystals (l) have a bigger band gap energy than larger crystals (r). [30]

2.3. Energy states in quantum dots

The energy of an electron in a quantum dot can be crudely estimated by the approximation of a particle in a one dimensional box with infinite potential wells, using the time-independent Schrödinger equation [31]:

$$E = E_n = \frac{\hbar^2 n^2 \pi^2}{2ma^2} = \frac{h^2 n^2}{8ma^2}$$

E_n = energy of an electron
 n = state of the wave function
 m = mass of the particle
 a = length of the box

For a three dimensional particle in the box approximation, the results are very similar:

$$E_{n_x} = \frac{\hbar^2 n_x^2 \pi^2}{2ma^2}$$

$$E_{n_y} = \frac{\hbar^2 n_y^2 \pi^2}{2mb^2}$$

$$E_{n_z} = \frac{\hbar^2 n_z^2 \pi^2}{2mc^2}$$

$$E_n = E_{n_x} + E_{n_y} + E_{n_z}$$

For a sphere, the approximation can be written as followed [32]:

$$E_{n,l} = \frac{\hbar^2 \alpha_{n,l}^2}{2mr^2}$$

$\alpha_{n,l}$ = n^{th} zero of the l^{th} order Bessel function
 r = radius of the sphere

Louis E. Brus used this approximation to derive an equation, the Brus-equation, that shows the energy of a photon emitted by a quantum dot as a function of the band gap energy of the bulk material (E_g), the confinement effects of electrons and holes and the coulomb attraction between electron and hole. [33]

$$E_{QD}(r) = E_g + \frac{\hbar^2}{8r^2} \left(\frac{1}{m_e^*} + \frac{1}{m_h^*} \right) - \frac{1.8e^2}{4\pi\epsilon\epsilon_0 r}$$

E_{QD} = energy of an electron in a QD
 E_g = Bulk band gap energy
 r = radius of the QD
 m_e^* = effective mass of excited electron
 m_h^* = effective mass of excited hole
 ϵ = absolute permittivity
 ϵ_0 = vacuum permittivity

With this equation, the size of a quantum dot can be calculated by measuring the wavelength of the emitted photons. Furthermore, it is obvious that the discrete energy spacing for materials with a large radius (r) do not differ very much. However, when the radius gets small enough (less than the exciton Bohr radius [34]), the energy differences become such that quantum confinement effect become visible. One of the most well-known properties of the quantum confinement effect is the size-specific emission of photons by quantum dots (figure 6.).

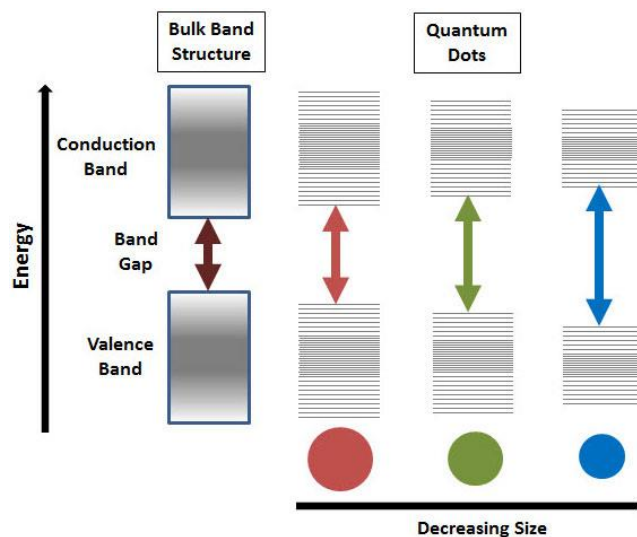


Figure 6. Band splitting for semiconductor materials of different sizes leads to size specific emission of photons. [35]

2.4. Electron excitation and photon emission of quantum dots

Quantum dots exhibit the quantum confinement effect which arises due to the discrete energy levels in a quantum dot, as elaborated before (2.2.). This leads to, amongst others, a size specific emission of photons when electrons in these quantum dots are excited by an incoming photon of higher energy (2.3.). The wavelength of these photons is determined by the radius of the particle and the bandgap energy of the semiconductor material (Brus-equation).

Photon stimulated excitation of an electron can be illustrated as in figure 7a. The generated hot electron and hole, also called exciton, usually cool down to the band edge, the conduction and valence band, by thermal relaxation as shown in figure 7b. The emission of photons by recombination of the electron and hole pair from a quantum dot can be depicted as shown in figure 7c.

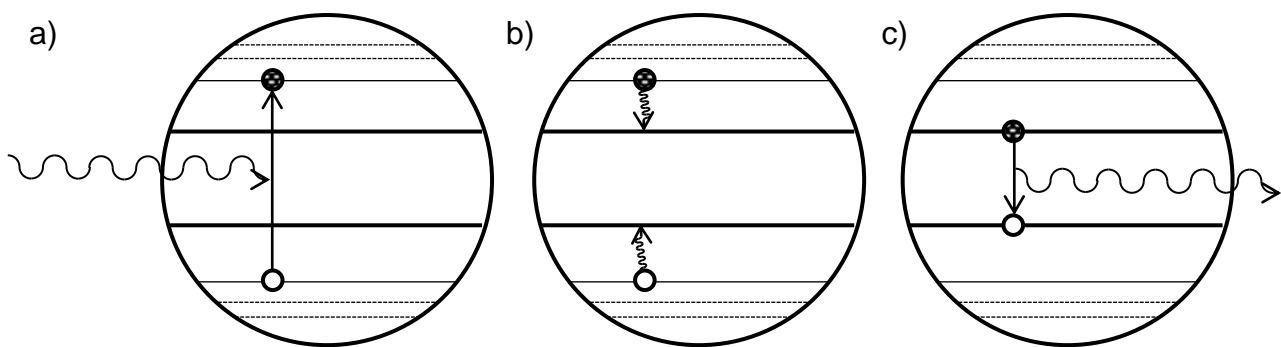


Figure 7. Photoexcitation (a), thermal relaxation (b) and emissive recombination (c) of an electron and a hole.

Impurities and undercoordinated atoms in the crystal, usually referred to as traps, lead to states inside of the band gap. This further leads to “conduction band to trap” or “trap to valence band” transitions, which are lower in energy. The spectrum of the emitted photons can thus be broadened in the case of impurities or structural defects in the quantum dots. Depending on the position of the trap state, the emission by a trap state can be depicted as figure 8a. for a trap state close to the conduction band, or as figure 8b. for a trap state close to the valence band.

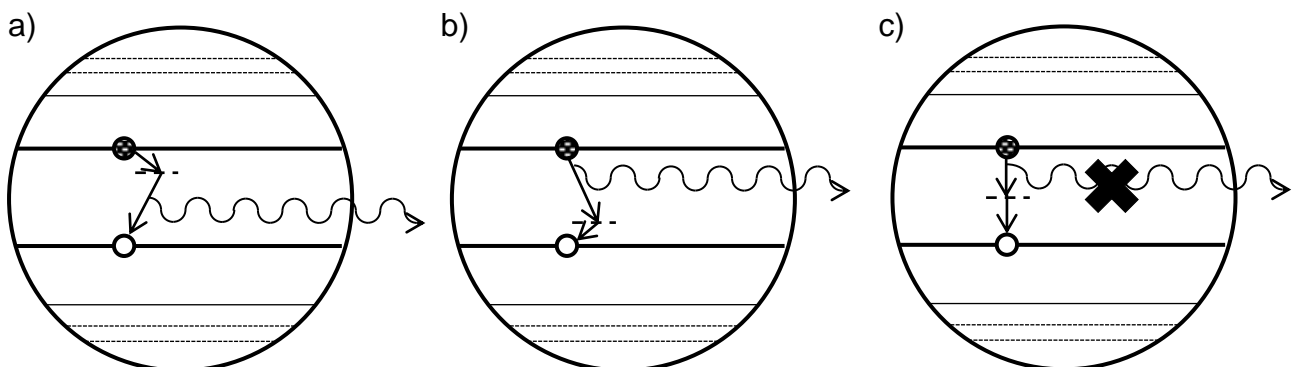


Figure 8. Trap state recombination for traps of different positions (a,b.). Some trap state recombination does not lead to the emission of a photon (c).

Trap state emission does not only broaden the emission spectrum significantly, it also reduces the photoluminescence quantum yield (PLQY) specific for the conduction to valence band transmission of the quantum dot. This is clearly visible by comparing the area of the emission peak and the area of the lower energy emission (figure 9.). The reduction is increased because not all trap state recombination leads to photon emission. Some energy is lost by phonon excitation or thermal relaxation (figure 8c.).

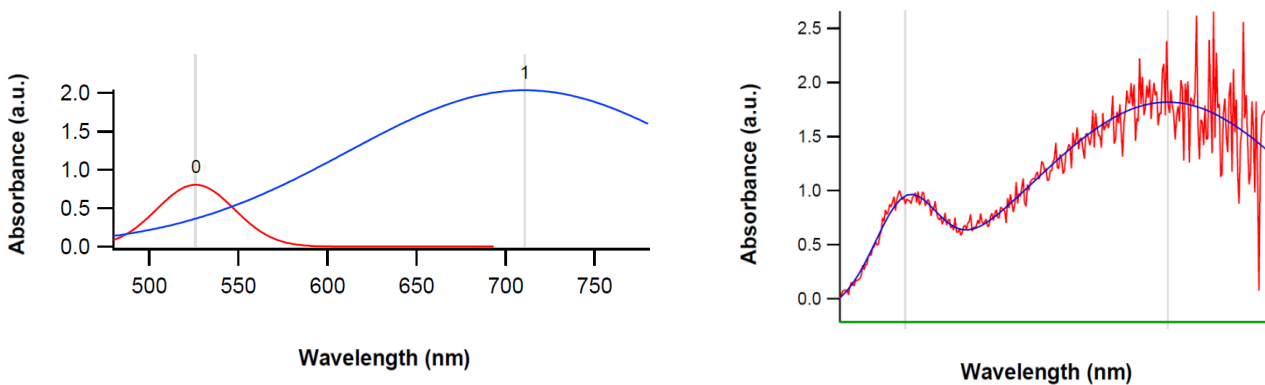


Figure 9. Band edge emission (l, red) and lower energy emission (l, blue) are combined in an emission spectrum (r), lowering the color purity.

The PLQY can furthermore be lowered by Auger electrons. In this special type of transmission, an electron and hole recombine, but instead of emitting a photon to lose the excess energy, the energy is transferred internal to create hot electrons and/or holes as shown in figure 10.

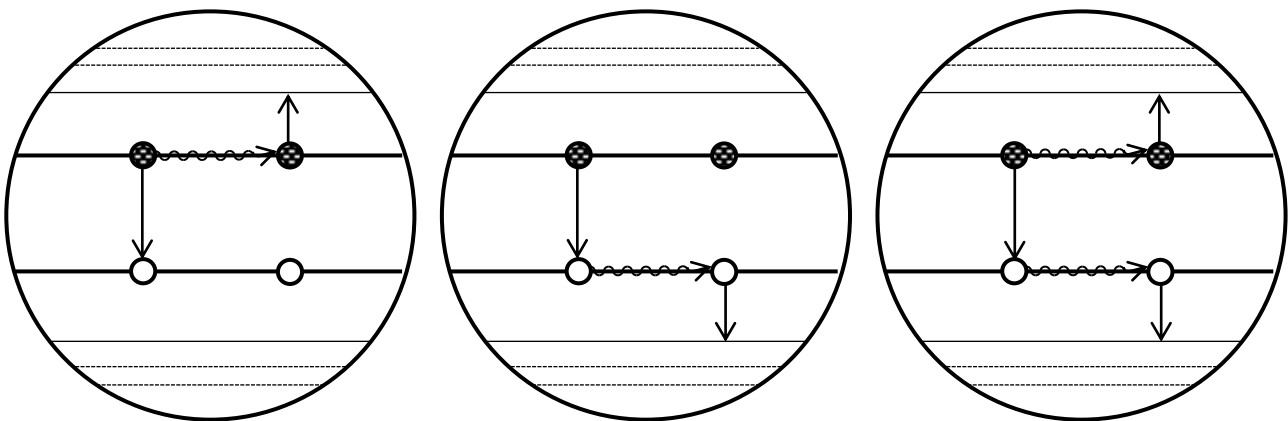


Figure 10. Different mechanisms for Auger recombination.

Instead of recombination from higher energy band (with the emission of a photon with a higher energy), the energy is most often lost due to thermal relaxation of the hot electron and/or hole to the band edge states as shown in figure 7b. for both the hot electron and hole. The loss of energy from the Auger electron leads to a lower PLQY, because the exciton decays without emission of a photon. Because Auger-electrons only become relevant at high light intensity or while charging quantum dots externally, they do not lower the PLQY for InZnP quantum dots in a significant way. Therefore, this is not treated further in this thesis.

2.5. The origin of structural defects

When crystals form from their precursor materials, atoms usually arrange in such a way that they gain enough electrons to fill each valence shell completely (according to the octet rule). For indium phosphide, all atoms inside of the crystal follow this rule, to be in the lowest energetic state. Atoms that reside on the surface of the crystal, however, cannot be fully coordinated. This phenomenon also occurs when there are mismatches inside of the crystal itself (in case of a vacancy or an interstitial atom in the crystal lattice), or when impurities are introduced in the crystal structure. Impurities and undercoordinated atoms in the crystal are the main cause for a lowered PLQY and emission broadening of InZnP quantum dots due to recombination in trap states. This happens, because the unpaired electrons and holes in both the undercoordinated atoms and impurities become spots for an excited electron and hole to recombine (figure 11.). These recombination states lie in between the conduction and the valence band, therefore leading to broadening of the emission and loss of PLQY.

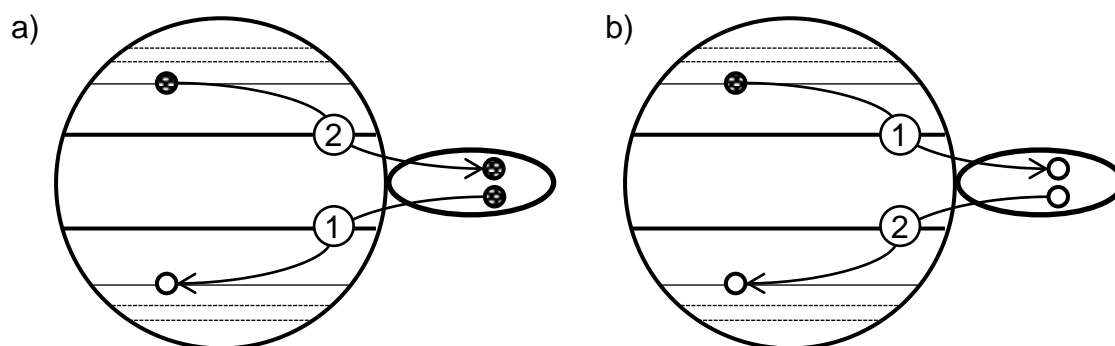


Figure 11. Recombination pathways in filled (a) and empty atomic orbitals (b).

2.6. Possible solutions for removing trap states

Trap states caused by vacancies and lattice disorders are generally difficult to remove, because they are normally inside of the crystal lattice. High purity precursors are therefore essential to synthesise quantum dots of a good quality. Atomic mismatches in quantum dots can be removed (partially) by annealing the quantum dots at a high temperature. In this way, for e.g. cadmium selenide, the PLQY and color purity increase significantly. [36] The atomic bonding of indium phosphide quantum dots however, has a much more covalent character than the ionic character of cadmium selenide bonds, hence annealing indium phosphide quantum dots requires a much higher temperature. The temperature range required is out of the limit of most practical solvents ($>500^{\circ}\text{C}$). [37] For indium phosphide quantum dot synthesis, the reaction should therefore be better controlled at the start.

Dangling bonds on the surface exist for each type of quantum dots. These dangling bonds can however easily be passivated in two ways. The first approach is to bind an appropriate ligand to the electron of the dangling bond. In this way, the recombination centres no longer exist. The second method is by growing an epitaxial shell of a higher band gap material around the quantum dot, also binding electrons of the dangling bonds, hence removing the recombination centres.

During quantum dot synthesis, organic ligands are already added to the reaction mixture, to reduce the growth rate of the quantum dots, decreasing the polydispersity of the sample. These ligands are however not bound strongly enough to the quantum dot surface. To ensure that the ligands don't come off when the ligand concentration in the solvent lowers (due to purification steps), these ligands need to be replaced in order to form a stable passivation layer. When choosing for ligand passivation, there are three ligand types (figure 12.).

X-type ligands are negatively charged ligands such as carboxylates, thiolates and halides, that can accept one electron to form a cation. L-type ligands are neutral Lewis bases such as amines and thiols, donating two electrons to an undercoordinated cation. The third type of ligands are Z-type ligands, which are Lewis acids such as metal salts or BF_3 , which can bind to a lone pair on an undercoordinated anion. [38]

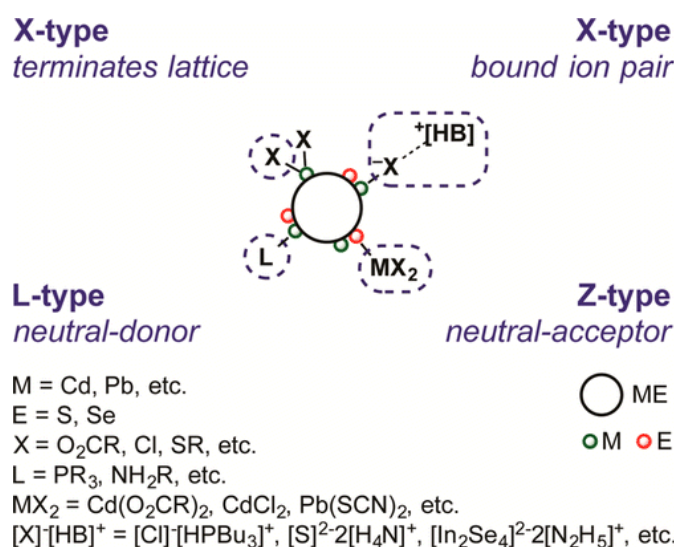


Figure 12. Different ligand types, that can be used to passivate the quantum dot surface. [38]

A layer of ligands can significantly reduce the recombination by trap states, however the layer of material can be easily removed due to an equilibrium between ligands on the surface and ligands in solution. Because indium phosphide is reactive towards moisture and oxygen from the air, a better passivation alternative for this type of quantum dots is an epitaxial shell. There are a few extra cautions by selecting the right shell material. First of all, the lattice parameters and crystal structure of the shell material should match the core material. Furthermore, the bandgap energy of the shell material needs to be higher and the band alignment for electrons and holes should be a type I structure (figure 13.). This, in order to keep both the electrons and the holes confined in the core. Only in this way, the broadness of the emission peak, typically determined by the full width half maximum (FWHM) of the emission, is kept low.

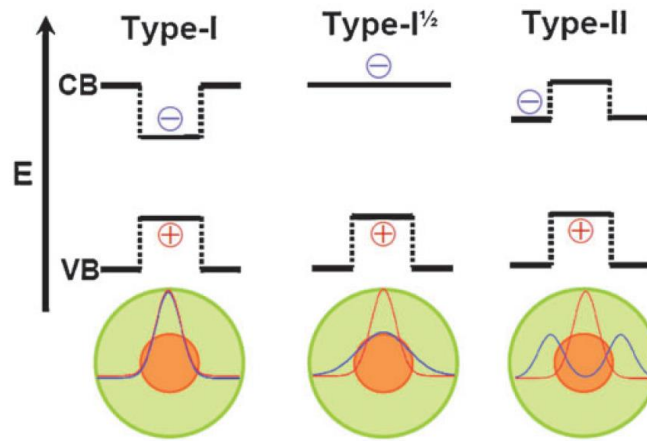


Figure 13. Different band alignments. Note that the band gap of a shell material should be a wide band gap semiconductor with a type I structure to keep both the holes and electrons confined in the core. [39]

From a chart with semiconductor materials, it can be seen that materials such as zinc selenide and magnesium selenide are good shell materials in the sense that they both are large band gap materials with a type I band alignment. A material as cadmium sulfide, type 1.5 (where the conduction bands are almost equal in energy, figure 13.), appears to be less useful (figure 14.) due to delocalization of the electron in both the core and shell.

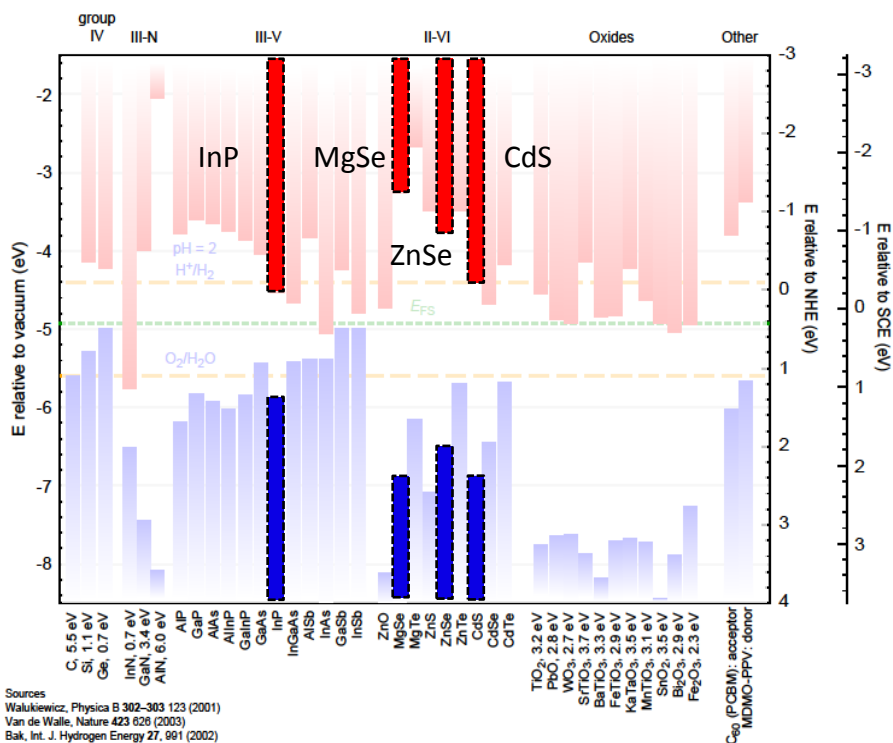


Figure 14. Different band alignments. Note that the band gap of a shell material should be a wide band gap semiconductor with a type I structure to keep both the holes and electrons confined in the core. [40]

In order to apply this theory in practice, in the next section the chemistry of quantum dot synthesis is elaborated to determine synthetic parameters. It ends with a selection for the best shell material to put around InZnP quantum dots.

2.7. Thermodynamics of quantum dot synthesis

Quantum dot synthesis is determined by four specific synthetic regions, which all should be optimal in order to produce quantum dots of high quality. These regions are (1) the initiation of the reaction, (2) the nucleation of crystals, (3) the growth of crystals and (4) Ostwald ripening. The first three regions are displayed in figure 15. Ostwald ripening is an effect that occurs during every region, however it gets more evident after long growth times.

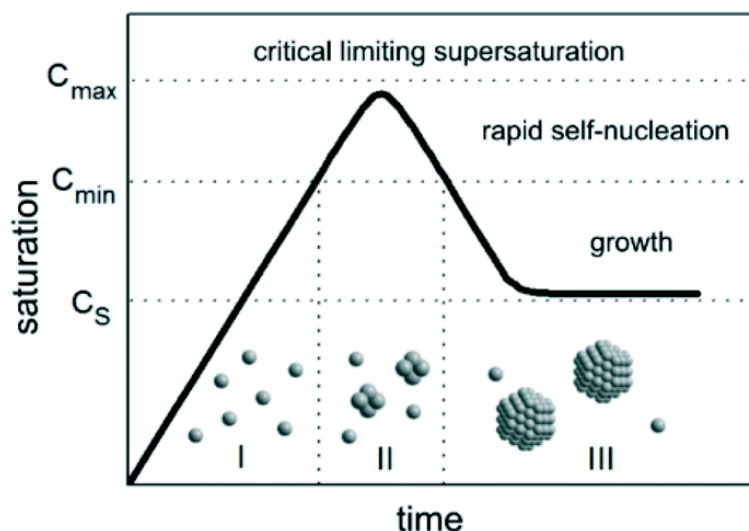


Figure 15. A schematic depiction of the initiation (I), nucleation (II) and growth (III) of quantum dots, as a function of saturation over time. [41]

The synthesis of quantum dots starts by the formation of seed crystals in solution. Seed crystals form regularly by random interactions of multiple monomers in solution, however these seed crystals normally dissolve rapidly again. To initiate the formation of many crystals in solution without redissolving, the concentration of the precursors should exceed the point of supersaturation.

Supersaturation alone, however, is not enough to induce nucleation of nanocrystals for high quality specimens. For nucleation, it is important that the seed crystals can reach the critical nucleus size. When this is not the case, the seed crystals rapidly dissolve again. To be able to grow crystals that are larger than the critical nucleus size, the change in free energy for the formation of clusters from monomers should be negative.

As can be seen from the equation and figure 16, the change in free energy for the formation of clusters from monomers is positive for very small particles, due to a predominant surface energy term. This is caused by a relatively high surface over volume ratio for small particles. This means that there is an activation energy for the formation of nuclei, dependent on the radius of the nanocrystal. This activation energy can be calculated once the critical radius (r_c) of the nuclei is known.

$$\Delta G(r) = \frac{-4\pi r^3 kT\sigma}{3V_m} + 4\pi r^2 \gamma$$

ΔG = total Gibbs free energy

r = radius of the QD

T = temperature

σ = degree of supersaturation

V_m = monomer volume

γ = surface tension

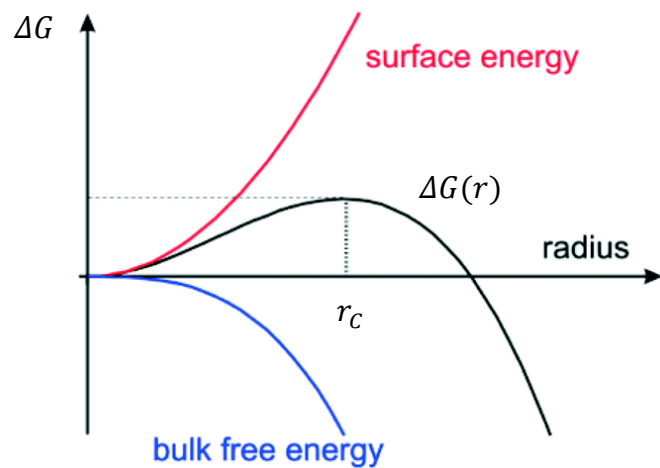


Figure 16. The function for the Gibbs free energy, and a schematic interpretation of the importance of both parts of the function. [41]

The critical radius size can be calculated by taking the derivative of the function for the free energy over the radius of the quantum dot and setting it to zero.

$$\frac{\Delta G(r)}{\partial r} = \frac{-4 \cdot 3 \pi r_c^2 kT\sigma}{3V_m} + 8\pi r_c \gamma = 0$$

$$= r_c \left(\frac{-4 \pi kT\sigma}{V_m} r_c + 8\pi \gamma \right) = 0$$

$$\frac{4 \pi kT\sigma}{V_m} r_c = 8\pi \gamma$$

$$r_c = \frac{2\gamma V_m}{kT\sigma}$$

The activation energy for the formation of nuclei therefore is:

$$\Delta G(r_c) = \frac{16}{3} \pi \gamma^3 \left(\frac{V_m}{kT\sigma} \right)^2$$

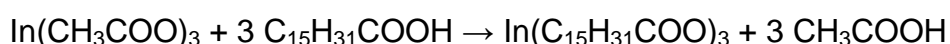
Because the monomer volume and surface energy are usually determined by factors which are difficult to control or modify, the easiest to overcome the activation energy barrier for nucleation is by changing the temperature and the concentration of the precursors.

To grow monodisperse batches of quantum dots from nuclei, the type of growth is very important. Depending on the concentration of precursors present, the growth is either dependent on the diffusion from the precursors to the surface of the nucleus (when the concentration of precursors is relatively low), or dependent on the kinetics of the growth (when the concentration of precursors is relatively high). Diffusion limited growth leads to size focussing, where the size distribution of the nuclei decreases. This phenomenon occurs due to the fact that larger nuclei need more material to grow a layer than smaller nuclei. Due to fact that diffusion of the precursors is limited, on average the same amount of precursors get to each nucleus, hence the size distribution decreases. For kinetically limited growth, there is enough material for each quantum dot to grow. This means that the rate of growing a new shell on a nucleus is the same for each nucleus, small or large, hence for kinetically limited growth, there is no size-focussing. Therefore, the concentration of the monomers should be high, but not too high, in order to get to the desired supersaturation lever for initiation and nucleation, but still be in the diffusion limited growth region during the quantum dot growth.

When quantum dots are grown for too long, smaller quantum dots can start to donate monomers to larger quantum dots. This occurs due to the lowering of the overall surface energy, which is thermodynamically favourable. Because smaller quantum dots decrease in size, and larger quantum dots increase in size, this is an unwanted effect that drastically increases the size distribution of the quantum dot batch. Therefore, the synthesis should be monitored, to make sure the effects of Ostwald ripening do not significantly influence the synthesis.

2.8. InP quantum dot synthesis

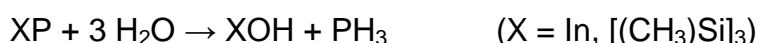
There are two common methods to produce InP quantum dots. First of all the hot-injection method, where the phosphorus precursor is injected in a hot solution of metal precursors. Secondly, there is the heating-up method, where all precursors are added at room temperature and the temperature is subsequently risen. These methods will be compared in chapter 4., but the chemistry of both syntheses is similar. First of all, the metal precursors are prepared. By a metathesis reaction, indium palmitate is made from indium acetate and palmitic acid. Under vacuum and heating, the acetic acid is removed:



Thereafter, tris(trimethylsilyl)phosphine ($\text{P}(\text{TMS})_3$) is injected, to react with the indium palmitate to form InP and side products as followed:



The reaction and the InP quantum dots should be handled with oxygen- and water free techniques to prevent side reactions like the following from happening:



These side reactions are potentially very dangerous, because $\text{P}(\text{TMS})_3$ is pyrophoric and phosphine (PH_3) is extremely toxic. Therefore, these syntheses are typically carried out using a glovebox and air free Schlenk lines in a fume hood.

2.9. Positive effects of Zn

In current InP syntheses, zinc salts are often added to decrease the size distribution or full width at half maximum (FWHM) from InP quantum dots. During the synthesis, zinc has a stabilizing role. [42] While the intermediates of the reaction between indium palmitate and $P(TMS)_3$ are unstable, hence a fast, uncontrolled reaction, the reaction intermediate between zinc salts and $P(TMS)_3$ is much more stable. This leads to a slow, controlled reaction and a far better FWHM. [42]

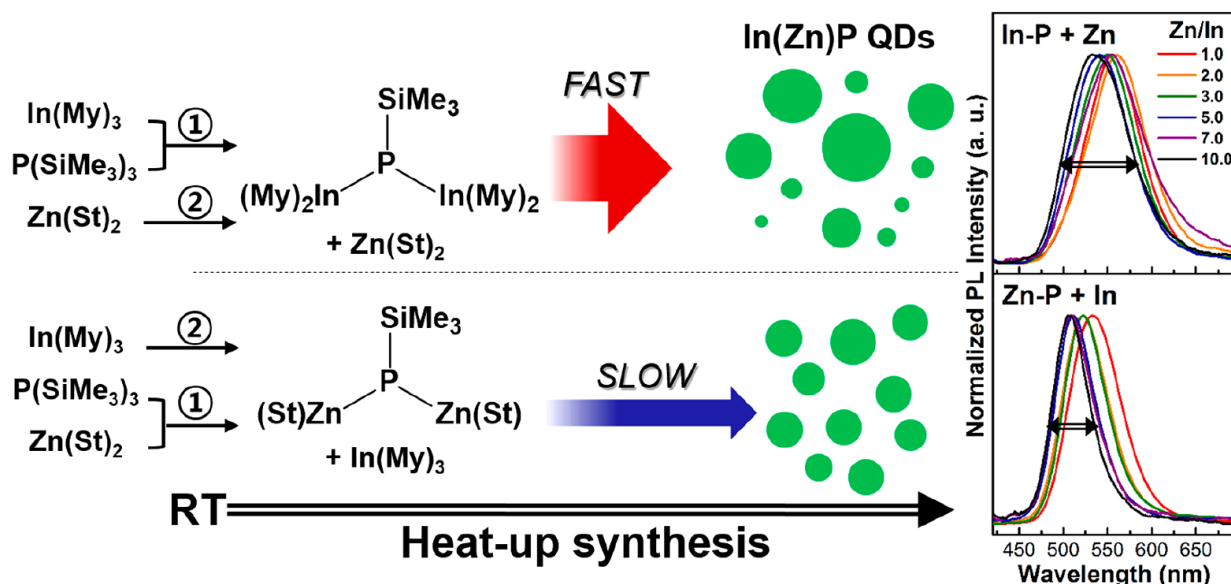
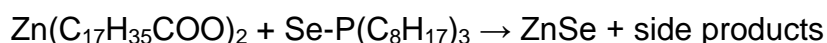


Figure 17. Zinc ions help to stabilize the phosphine complex, therefore reducing the growth rate. This leads to a more monodisperse size distribution of the sample. [42]

2.10. Shell growth around InZnP quantum dots

As previously explained, trap states can be passivated by binding ligands to dangling bonds or by growing an epitaxial shell around the quantum dot. Because especially organic ligands are too weakly bound to the surface of the quantum dot, attaching ligands is not the best choice for these quantum dots. Furthermore, by growing an epitaxial shell around the quantum dots, moisture and oxygen can be kept out. Growing an epitaxial shell around InZnP quantum dots is therefore the best option. Not only to increase the PLQY, but also to improve the stability of the QDs.

Commonly, zinc sulfide and zinc selenide are chosen to grow a shell around InZnP quantum dot cores. The material is grown by adding zinc and sulfur or selenium precursors to freshly synthesized InZnP cores. Mainly zinc stearate and trioctylphosphine-selenide are used for the synthesis of ZnSe. The reaction goes according to:



2.11. Reasoning and aim of the thesis

The main problem of ZnS and ZnSe as shell materials around InZnP quantum dot cores is that the lattice match between the core and the shell is not perfect. Therefore, dangling bonds will remain on the surface between the InZnP core and the ZnSe shell (figure 18.). The passivation thereby is not perfect, hence the PLQY is not as high as possible.

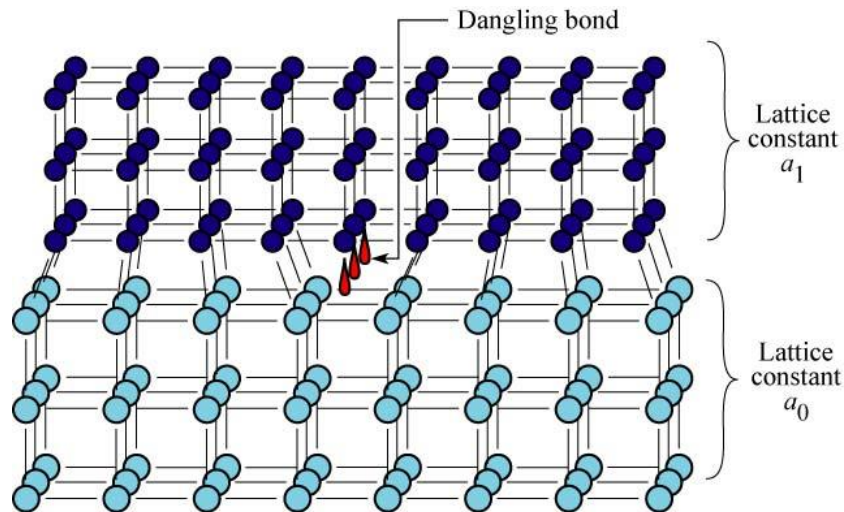


Figure 18. Dangling bonds created by the lattice mismatch between the core and the shell material of the quantum dot. For InP/ZnSe, InP has lattice constant a_0 and ZnSe a_1 . [43]

In order to find a material with a better matching lattice constant, one has to take into account that the other properties of the material should also match. The most important properties are the crystal structure, the band gap energy of the shell material and the type of semiconductor structure between the shell material and the InZnP core.

By taking all these parameters into account, magnesium selenide seemed to be the most promising material, as shown in table 1. The lattice constant matches the InZnP better, the crystal structure is zinc blende, as well as InZnP and the band alignment is a type I (see section 2.6.)

Table 1. Material properties of various potential shell materials for indium phosphide quantum dots, including the properties of indium phosphide.

Material	Lattice constant (Å)	Lattice mismatch with InP	Crystal structure	Band gap (eV)	Band alignment with InP
ZnS	5.41 [44]	- 7.8%	Zinc blende [44]	3.68 [44]	Type I
ZnSe	5.67 [44]	- 3.4%	Zinc blende [44]	2.82 [44]	Type I
InP	5.87 [45]	-	Zinc blende [45]	1.34 [45]	-
MgSe	5.90 [46]	0.51%	Zinc blende [46, 47]	4.05 [46, 47]	Type I
MgSe	5.46 [46]	- 7.0%	Rock salt	3.5 [48]	Type I

The main problems of MgSe as a shell material is that, first of all, MgSe has the rock salt structure as its native crystal structure, and not the desired zinc blende. By incorporating zinc selenide in the material, hence making a $Zn_xMg_{1-x}Se$ alloy, the crystal structure should be zinc blende. Furthermore, according to DFT calculations the lattice match is better for $Zn_xMg_{1-x}Se$ than for MgSe (table 2.). [49] For the rest of this thesis, $Zn_xMg_{1-x}Se$ will be abbreviated to ZnMgSe.

Table 2. Calculated lattice constants for different fractions of magnesium in ZnMgSe, as well as InP and ZnS for comparison.

Material	Lattice constant (Å) (calculated)	Lattice mismatch with InP (calculated)
InP ²	5.87	-
ZnSe	5.738	- 2.2%
Zn _{0.75} Mg _{0.25} Se	5.815	- 0.90%
Zn _{0.50} Mg _{0.50} Se	5.877	0.15%
Zn _{0.25} Mg _{0.75} Se	5.938	1.2%
MgSe	6.002	2.3%
ZnS	5.465	- 6.9%

² InP was not calculated, but taken as reference from [45].

A second problem is posed by the reactivity of magnesium selenide. MgSe is prone to hydrolysis and oxidation according to the following reactions:



The easiest solution to this problem is to add a protective, second shell around the core-shell quantum dot, to make a core-shell-shell structure. The material chosen for this second shell layer is zinc sulfide, because it is stable and unreactive towards water and oxygen and it has the same crystal structure (zinc blende) as ZnMgSe.

The aim of this thesis is to synthesize InZnP quantum dots with a narrow FWHM and a high PLQY. This should be performed by selecting the best core synthesis method and thereafter passivating the surface of these quantum dots with a lattice matched ZnMgSe shell. This shell material should thereafter be protected by a thick ZnS shell to protect the material against negative influences from the exterior. When successful, these InZnP/ZnMgSe/ZnS core-shell-shell quantum dots can be a less toxic alternative to the now commonly used cadmium based quantum dots such as cadmium selenide.

3. Experimental work

In the coming chapters, the results of the experiments performed for this thesis are treated. For all the results obtained, the chemicals and equipment mentioned below are used. All the general synthetic protocols used for this thesis can be found in sections 3.3. to 3.8.

All the results in this thesis are obtained under the supervision of Dr. N.R.M. Kirkwood.

3.1. Used chemicals

Methyl acetate (anhydrous, 99.5%); methanol (anhydrous, 99.8%); toluene (anhydrous, 99.8%); 1-octadecene (ODE) (technical grade, 90%); tetracosane, (99%); tris(trimethylsilyl)phosphine (PTMS) (95%); tributylphosphine (TBP) (mixture of isomers, 97%); trioctylphosphine (TOP) (97%); trioctylphosphine oxide (TOPO) (ReagentPlus®, 99%); selenium (99.99%); palmitic acid (HPA) (>99%); sodium palmitate (NaPA) (98.5%); gallium chloride (anhydrous, 99.99% trace metal basis); indium acetate ($\text{In}(\text{OAc})_3$) (99.99% trace metal basis); zinc acetate ($\text{Zn}(\text{OAc})_2$) (99.99% trace metal basis); zinc stearate (ZnST) (technical grade); diethylzinc ($\geq 52\text{wt.}\%$ Zn basis); magnesium stearate (MgST) (technical grade) and dibutyl magnesium (1M in heptane) were purchased from Sigma-Aldrich. Ethanol (absolute, SupraSolv® for GC-EDC/FID) was purchased from Merck. Oleylamine (OLA) (80-90% C18, $\geq 96.0\%$ (primary amine)) was purchased from Acros Organics. n-Hexane (anhydrous); sulfur (Puratronic®, 99.9995%); were purchased from Alfa Aesar.

Indium palmitate (InPA) and zinc palmitate (ZnPA) were prepared as discussed in section 2.8, using sodium palmitate (NaPA) and indium or zinc acetate respectively.

Note that all the solvents and precursors need to be prepared, handled and combined under an inert atmosphere, unless stated differently. Any oxygen or water present will react with the precursors and the quantum dots, potentially creating harmful situations and decreasing the quality of the quantum dots. Therefore, it is best to do the synthesis preparations and quantum dot washing steps in a nitrogen filled glovebox, while using anhydrous solvents. The reaction itself can be carried out on a Schlenk line that is completely filled with dry nitrogen gas. For all the reactions performed in the thesis, the nitrogen (5N) from the Schlenk line was dried over a column filled with phosphorus pentoxide as desiccant.

3.2. Used equipment

For the absorption spectrophotometry, a Perkin-Elmer Lambda 40 UV/Vis spectrometer was used. For the emission spectrophotometry, an FLS980 fluorescence spectrometer from Edinburgh Instruments Ltd. was used. A JEOL JEM1400 transmission electron microscope, operating at 120 keV was used to make TEM images, as well as for obtaining energy-dispersive X-ray spectroscopy (EDX) and electron diffraction (ED) data.

3.3. Hot injection synthesis of InZnP core QDs

This synthetic method is adapted from Pietra *et al.* [50]

7 mL ODE, 106 mg InPA (0.12 mmol) and 34 mg ZnPA (0.06 mmol) were added to a 25 mL three necked flask. The mixture was degassed at a high vacuum (<0.2 mbar) at 140°C for 2 hours. Subsequently, the mixture was heated to 300°C. While vigorously stirring, 17 µL PTMS (0.06 mmol) dissolved in 1 mL ODE was injected and the reaction mixture was cooled down to 270°C. The mixture was left to react until the desired size was reached. When the desired size was reached, the mixture was cooled back to 80°C. Subsequently, 4 mL toluene was added to the mixture.

In a glovebox, methyl acetate was added, until the solution turned turbid. Thereafter, the mixture was centrifuged at 1800 rcf for 5 minutes, the supernatant was decanted off and the quantum dot precipitate was redissolved in 1 mL toluene. This washing step was performed twice more and the final quantum dots were stored in 1 mL toluene under inert atmosphere.

3.4. Heating-up synthesis of InZnP core QDs

This synthetic method is adapted from Ramasamy *et al.* [51]

5 mL ODE, 44 mg In(OAc)₃ (0.15 mmol), 14 mg Zn(OAc)₂ (0.075 mmol) and 147 mg HPA (0.575 mmol) were added to a 25 mL three necked flask outside of the glovebox. The flask was attached to a Schlenk line. A vacuum of <0.2 mbar was applied overnight, while heating to 120°C. The next day, the flask was put under dry nitrogen and cooled back to 50°C. Subsequently, 29 µL PTMS (0.1 mmol) dissolved in 1 mL TOP was injected and the mixture was heated to 305°C with steps of 5°C per 20 seconds. When the mixture reached 305°C, it was stirred for 2 minutes at this temperature and then rapidly cooled down to below 80°C. Thereafter, 3 mL toluene was added.

In a glovebox, ethanol was added, until the solution turned turbid. Thereafter, the mixture was centrifuged at 1800 rcf for 5 minutes, the supernatant was decanted off and the quantum dot containing oil that was left on the bottom was redissolved in 1 mL hexane.

3.5. InZnP/Zn(Mg)Se/ZnS synthesis (stearate precursors)

This synthetic method is adapted from Ramasamy *et al.* [51] The main difference is the use of washed cores (section 5.1.). Various fractions of Zn:Mg were used (table 3.).

1 mL washed cores, synthesized as in section 3.4., was added to 10 mL (degassed) ODE in a 25 mL three necked flask, connected to a Schlenk line. A high vacuum <0.2 mbar was applied for 30 minutes, while the mixture was heated to 50°C. Thereafter, the mixture was rapidly heated to 300°C. At 70°C, 0.05 mmol metal stearates suspended in 1 mL ODE was injected. At 300°C 150 µL 1M TOP-Se in TOP (0.15 mmol) dissolved in 100 µL TOP was injected and left to react for 15 minutes. Subsequently, 0.1 mmol metal stearates suspended in 1 mL ODE was injected and left to react for 10 minutes. Then, 100 µL 1M TOP-Se in TOP (0.1 mmol) dissolved in 100 µL TOP was injected and left to react for 15 minutes. The last two steps were repeated once more, to grow an additional Zn(Mg)Se

shell layer. 10 minutes after the last addition of metal stearates, the mixture was cooled down to 80°C and 4 mL of toluene was added.

To the quantum dots, a 1:1 mixture of ethanol and methyl acetate was added until the solution turned turbid. The mixture was centrifuged at 1800 rcf for 5 minutes, the supernatant was decanted off and the quantum dot precipitate was redissolved in 1 mL toluene. This washing step was performed twice more, but by using only methyl acetate and the final quantum dots were stored in 1 mL toluene under inert atmosphere.

Table 3. The mass of the metal stearates used for shells with different fractions of Zn:Mg.

Zn:Mg	ZnST (mg)	ZnST (mmol)	MgST (mg)	MgST (mmol)
1:0 (100%:0%)	63	0.1	0	0
19:1 (95%:5%)	60	0.95	3	0.005
9:1 (90%:10%)	57	0.9	6	0.01
4:1 (80%:20%)	50	0.8	12	0.02
3:1 (75%:25%)	47	0.75	15	0.025
1:1 (50%:50%)	32	0.05	30	0.05
0:1 (0%:100%)	0	0	59	0.1

3.6. Zn(Mg)Se synthesis (stearate precursors)

This synthetic method is adapted from Li *et al.* [52] Various fractions of Zn:Mg were used (table 4.).

To a 25 ml three necked flash, 4g ODE (5.08 mL) and 0.1 mmol metal stearates were added. A vacuum of <0.2 mbar was applied and the flask was heated to 150°C for 1.5 hours. Subsequently the flask was filled with nitrogen and then heated to 325°C and 48 mg selenium powder (0.6 mmol) dissolved in 243 µL TBP and 380 µL ODE was injected. When the desired size was reached, the mixture was cooled down rapidly to 80°C and 1mL toluene was added.

To the mixture, ethanol was added under inert atmosphere until the solution turned turbid. The solution was subsequently centrifuged at 1800 rcf for 5 minutes, the supernatant was decanted off and the precipitate was redissolved in 1 mL toluene. This washing step was performed once more, but by using methyl acetate instead of ethanol. The final product was stored in 1 mL toluene under inert atmosphere.

Table 4. The mass of the metal stearates used for nanoparticles with different fractions of Zn:Mg.

Zn:Mg	ZnST (mg)	ZnST (mmol)	MgST (mg)	MgST (mmol)
1:0 (100%:0%)	63	0.1	0	0
3:1 (75%:25%)	47	0.75	15	0.025
1:1 (50%:50%)	32	0.05	30	0.05
1:3 (25%:75%)	16	0.025	44	0.075
0:1 (0%:100%)	0	0	59	0.1

3.7. Zn(Mg)Se synthesis (organometallic precursors)

This synthetic method is adapted from Boldt *et al.* [53] Various fractions of Zn:Mg were used (table 5.).

8.61 mL (7g) OLA was heated in a 25 mL three necked flask to 300°C. Subsequently, 785 µL 1M TOP-Se in TOP (0.785 mmol) dissolved in 1.60 mL TOP was injected. Directly afterwards, 0.785 mmol of organometallic precursors was added. Note, the two metal precursors should not be mixed, prior to injection. After 30 minutes, 245 µL 1M TOP-Se in TOP (0.245 mmol) dissolved in 0.50 mL TOP was injected. Directly afterwards, 0.245 mmol of organometallic precursors was added. After 30 minutes, the temperature was lowered to 200°C and subsequently 1 mL diethylzinc (1mmol) and 1 mL 1M TOP-S in TOP (1 mmol) were added by a syringe pump over the course of 2 hours. These precursors were added together in one syringe. After the injection was completed, the mixture was stirred for 30 minutes to anneal any defects. The final mixture was washed with ethanol, by adding ethanol until the solution went turbid. The turbid solution was centrifuged and the precipitate was redissolved in 1 mL toluene. This was done once more, and thereafter the sample was stored under inert atmosphere.

Table 5. The volume of organometallics used for nanoparticles with different fractions of Zn:Mg.

Zn:Mg	1M Zn(Et) ₂ (mL)	Zn(Et) ₂ (mmol)	1M Mg(Bu) ₂ (mL)	Mg(Bu) ₂ (mmol)
1:0 (100%:0%)	0.245	0.245	0	0
3:1 (75%:25%)	0.184	0.184	0.061	0.061
1:1 (50%:50%)	0.123	0.123	0.123	0.123
0:1 (0%:100%)	0	0	0.245	0.245

3.8. InZnP/Zn(Mg)Se/ZnS synthesis (organometallic precursors)

For this synthesis, no procedure existed. The reasoning behind the steps can be found in section 9.2. Various fractions of Zn:Mg were used (table 6.).

1 mL washed cores, synthesized as in section 3.4., was added to a mixture of 5 mL ODE and 5 mL OLA in a 25 mL three necked flask, connected to a Schlenk line. A high vacuum <0.2 mbar was applied for 30 minutes, while the mixture was heated to 50°C. Thereafter, the mixture was rapidly heated to 200°C. At the same time, by using syringe pumps, add 0.35 mL 1M TOP-Se in TOP (0.35 mmol), 0.3 mL TOP and 0.2 mmol organometallic precursors to the mixture over the course of 1 hour. Next, the mixture was heated to 240°C and 1.6 mL of TOP-S (1.6 mmol) and 1.6 mL of diethylzinc (1.6 mmol) were added by a syringe pump at a rate of 2.5 mL per hour (1.25 mL per precursor).

After the addition was completed, the mixture was lowered to 80°C and 1.5 mL of toluene was added. For the first wash, 32 mL of methyl acetate was added to the solution. The total mixture was centrifuged at 1800 rcf for 5 minutes. The precipitate was redissolved in 2 mL of toluene and washed again by adding 6 mL of methyl acetate. The total mixture was centrifuged again at 1800 rcf for 5 minutes, and the precipitate was dissolved in 0.75 mL toluene. The samples were stored under inert atmosphere.

Table 6. The volume of organometallics used for shells with different fractions of Zn:Mg.

Zn:Mg	Zn(Et) ₂ (mL)	Zn(Et) ₂ (mmol)	Mg(Bu) ₂ (mL)	Mg(Bu) ₂ (mmol)
1:0 (100%:0%)	0.2	0.2	0	0
1:1 (50%:50%)	0.1	0.1	0.1	0.1

4. InZnP core synthesis methods

The aim of this chapter is to find the optimal conditions for the core synthesis to make a standard procedure for the rest of the syntheses. The two most important synthetic methods for making quantum dot cores with a monodisperse size distribution are the hot injection method (4.1.) and the heating up method (4.2.). To identify which method gives the best cores in terms of a low HWHM, the synthetic procedures of two recent research articles (one heating up method and one hot injection method) were reproduced and the synthesized cores were compared (4.3.).

4.1. Hot injection method

The hot injection method is based on the quick addition of the phosphorus precursor, a solution containing tris(trimethylsilyl)phosphine (PTMS) in octadecene (ODE) to the metal precursors (indium palmitate and zinc palmitate) which are heated to 300°C in ODE prior to the PTMS addition (figure 19.).

For the hot injection method, the research article of Pietra *et al.* (June 2017) was used (section 3.3.). [50] This synthesis method produced InZnP cores with an In:Zn ratio of 2:1 that were able to be grown to the preferred size as a function of reaction time (figure 20a.). By subsequent addition of more precursor materials to already grown cores, they can be grown larger (figure 20b.).

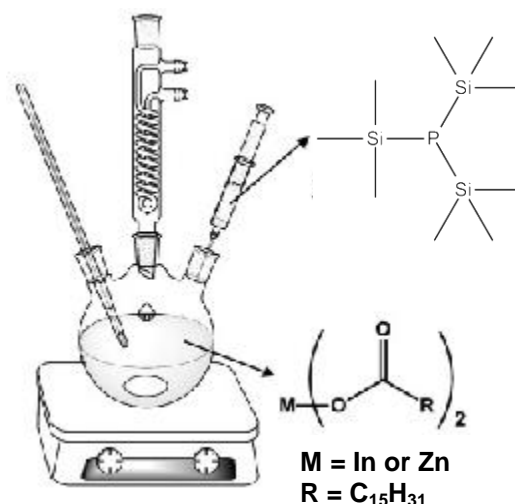


Figure 19. Reaction setup for the hot injection method. Prior to injecting the PTMS, the metal palmitates in ODE are heated to 300°C. Adapted from [54].

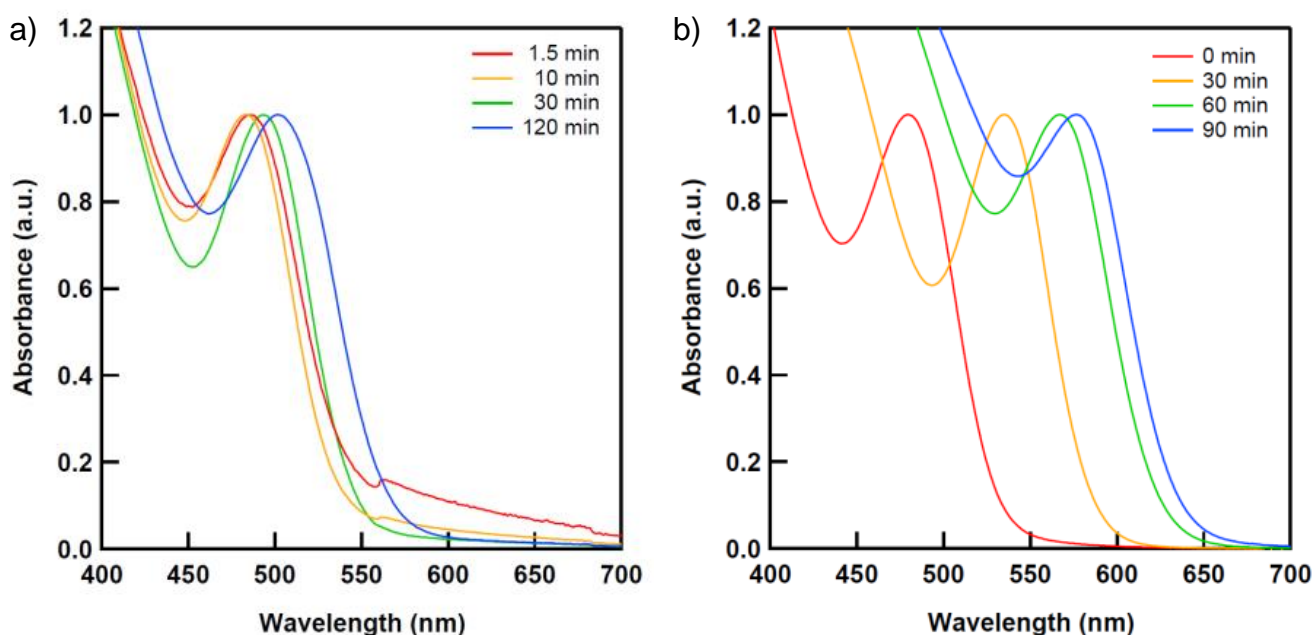


Figure 20. InZnP cores grown over time without (a) and with (b) subsequent addition of more precursor materials.

In order to further grow the cores by subsequent addition of precursors, the metal and phosphorus precursors have to be added separately. When combined, it was found that they prereact in the syringe, broadening the size distribution of the quantum dots (figure 21.).

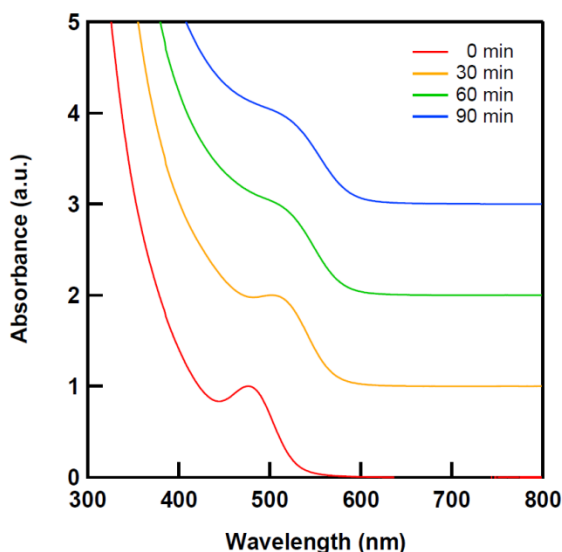


Figure 21. InZnP cores grown by subsequent addition of more precursor materials to already synthesized cores. The precursors for this reaction were combined in one syringe, showing growth and significant broadening over time.

Furthermore, changes in the precursor compositions sometimes have an influence on the formed cores. When replacing 1/3 of the ODE from the PTMS precursor solution for trioctylphosphine (TOP), which can act as a ligand, there is no significant change in the HWHM or the absorbance of the quantum dots (figure 22a.). But, when changing the In:Zn fraction to 1:1, cores with a much more blue-shifted absorption peak form, compared to cores with an In:Zn fraction of 2:1 (figure 22b.). This is caused by a decrease of the lattice parameters of the core. [55]

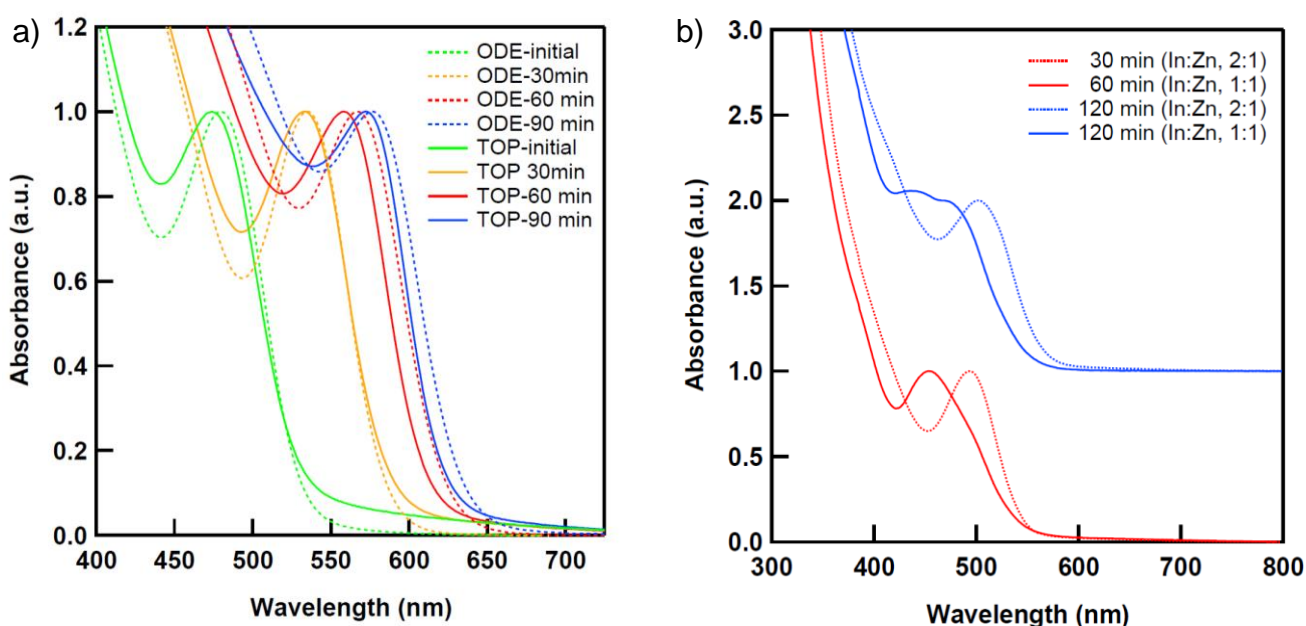


Figure 22. The effects of changes in precursor compositions for a partial substitution of ODE to TOP (a) and for a decreased indium to zinc ratio (b).

4.2. Heating up method

For the heating up method, both the metal and the phosphorus precursors are combined at room temperature and thereafter slowly heated to 300°C with a rate of 5°C/20s. Instead of premade metal palmitates (which are used for the hot injection method), metal acetates and palmitic acid are used, that in an overnight degassing step at 150°C under vacuum pressure (<0.2 mbar) form the metal palmitates with acetate residues left (although most acetate residues are boiled off as acetic acid). Furthermore, TOP is used instead of ODE for the PTMS precursor solution.

To make cores by the heating up method, the research article of Ramasamy *et al.* was used. [51] This synthesis method produced InZnP cores with an In:Zn ratio of 2:1, that, according to the article, are able to grow to the preferred size as a function of the palmitic acid (HPA) concentration. For this research, just one HPA concentration was used. This synthesis lead to cores with almost identical absorption peaks (figure 23a.). When replacing TOP from the PTMS precursor solution for ODE (as is normal for the hot injection method), there is significant broadening of the size distribution, hence a high HWHM of the absorbance of the quantum dots compared to the synthesis with TOP (figure 23b.).

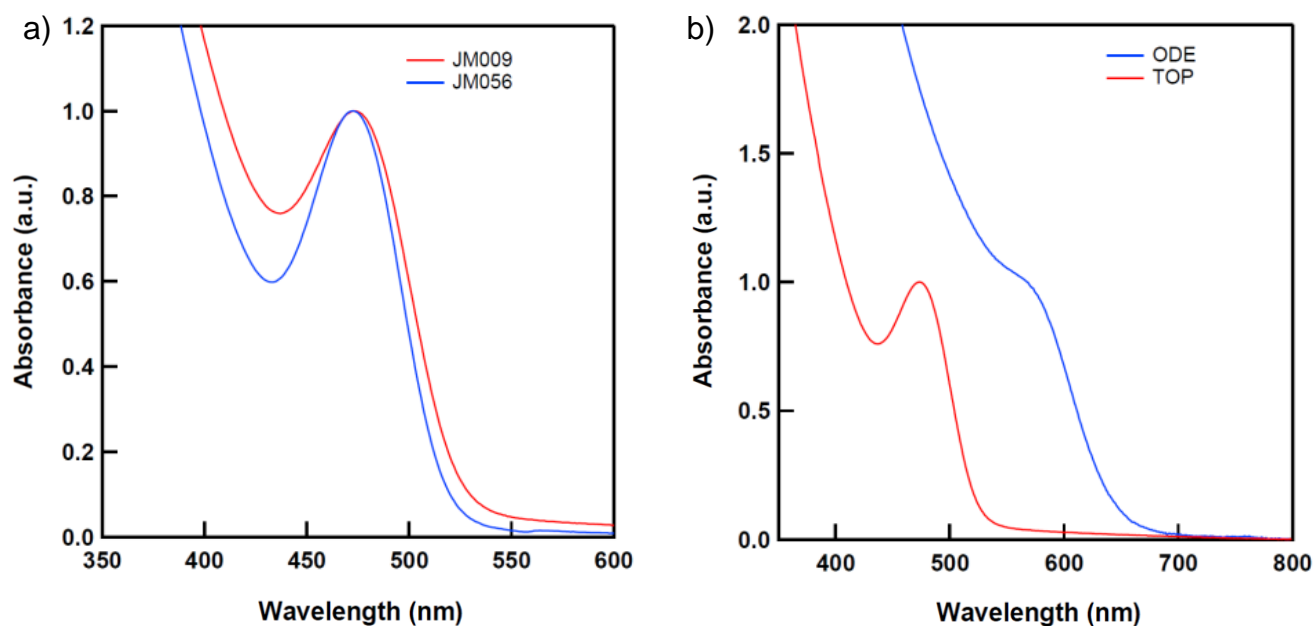


Figure 23. Two batches of InZnP cores, both grown by the heating up method show almost identical absorption peaks (a). They can however not be synthesized without TOP in the PTMS precursor solution (b).

4.3. Comparison of the two methods

From the results in table 6. and figure 24., it can be seen that the heating up method produces cores with a slightly better size distribution than the hot injection synthesis. Furthermore, in terms of reproducibility, the heating up synthesis is preferred, because the growth of the particles is determined by the concentration of palmitic acid (which solely depends on weighing the same amount of precursors every time), hence errors in timing are excluded. Also, errors that arise due to a difference in the way and swiftness of the injection do not have a notable influence in the heating up synthesis, whereas for the hot injection method this is of significant detail. The only downside of the heating up method is the longer waiting time due to the overnight degassing step.

Table 6. Comparison of the different core synthesis methods.

Batch number	Synthesis method	Absorption peak (nm)	HWHM (nm)
JM001	Hot injection	493	30
JM002	Hot injection	485	35
JM003	Hot injection	480	30
JM005	Hot injection	474	34
JM009	Heating up	472	30
JM056	Heating up	474	27

When comparing all the influencing factors and the results obtained, the heating up method was chosen to be the better one for the production of the InZnP quantum dot cores in the rest of this thesis.

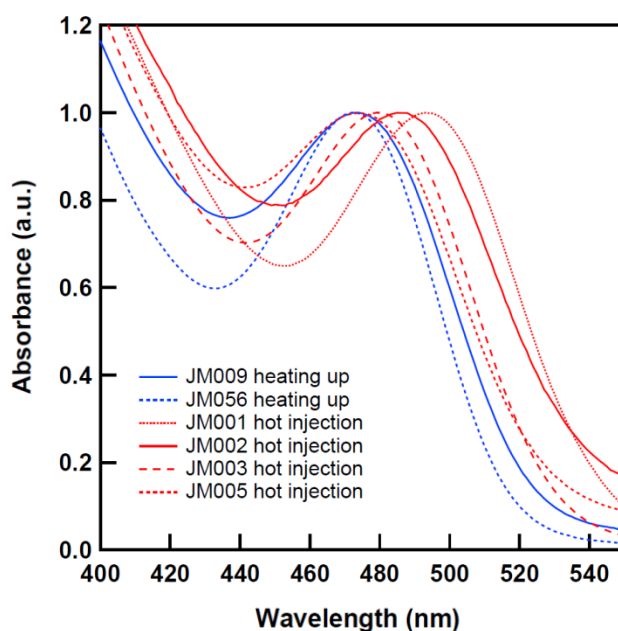


Figure 24. Comparison of different core synthesis batches. The heating up method appears to be more reproducible.

5. InZnP/ZnMgSe core – shell synthesis

Now the core synthesis method has been chosen (4.3.), shells can be grown around the synthesized cores. In section 5.1., there will be focused on the importance of purifying the cores prior to the shell synthesis. Thereafter, the importance of the first shell layer is explained (5.2.). The results of the synthesis of ZnMgSe shells containing various fractions of magnesium are discussed in section 5.3. In section 5.4., the issues with this synthesis method are explained.

5.1. Necessity of washing cores prior to shell synthesis

Cadmium based quantum dot cores are always washed (purified) before a shell is grown on them. [56] This has the advantages of removing unreacted precursors, as well as the ability of making a stock solution of quantum dot cores. However, indium phosphide quantum dot cores are never washed prior to shell growth in literature. [50, 51] To see what the effects of washing are to the quantum dots when growing a shell on them, an experiment was set up to compare washed and unwashed cores with a thin ZnSe shell on them.

A washing procedure was made that fits in between the core synthesis and the shell growth. The syntheses were performed simultaneously, to get the most reliable results. It includes adding toluene to the reaction mixture (QDs, precursors and ODE) to make it miscible with ethanol which is subsequently added. Ethanol is an antisolvent, hence the QD cores precipitate. By centrifuging the cores and discarding the supernatant (which includes the unreacted precursors), the purified cores remain as a solid on the bottom of the vial. Thereafter, the solid QDs are redissolved in hexane and can then be added back to fresh ODE, in order to grow shells around the cores.

The shell synthesis method comes from the article from Ramasamy *et al.* [51] where a zinc stearate suspension in ODE and TOP-Se, selenium powder reacted with TOP, are the precursors for the shell material. Both precursors are added dropwise to the reaction mixture, one after the other with time intervals of 10 and 15 minutes, to prevent nucleation of ZnSe particles.

From the absorbance and emission spectra (figure 25a., thick and thin lines respectively), the cores of both syntheses show a similar trend. The washing step does not influence the absorption and emission spectra of the cores, hence there is no negative influence of the washing step. When the first selenide shell is grown on the cores however, there is a notable red-shift for both quantum dots. The biggest difference obtained is that of the defect emission. The defect emission of the unwashed cores is substantial, and increases after each addition of selenium. For the washed cores, the defect emission is almost gone, and does not reappear on a large scale. Furthermore, the absorbance of the unwashed cores broadened significantly, compared to the washed cores, which resulted in a drastic color difference of the two batches (figure 25b.). This can be caused by secondary nucleation (as seen by the second peak in the the absorption spectrum of the cores with a full ZnSe layer), as well as by the formation of other materials by the reaction of unreacted precursors with the newly added precursors (e.g. a reaction between residual indium palmitate and TOP-Se).

5.2. The effects of a protective, passivating shell

In section 2.6. is explained that the shell layer binds to the under-coordinated atoms on the surface of the quantum dot core, thereby removing trap states. The fact that the dangling bonds are now filled energy states, should in theory lower the non-radiative recombination of the excitons significantly, because the recombination sites are no longer accessible. This can indeed be seen in figure 25a. The cores have a defect emission that is orders larger than the emission related to normal radiative emission from conduction band to valence band. This is mostly related to exciton recombination on the surface.

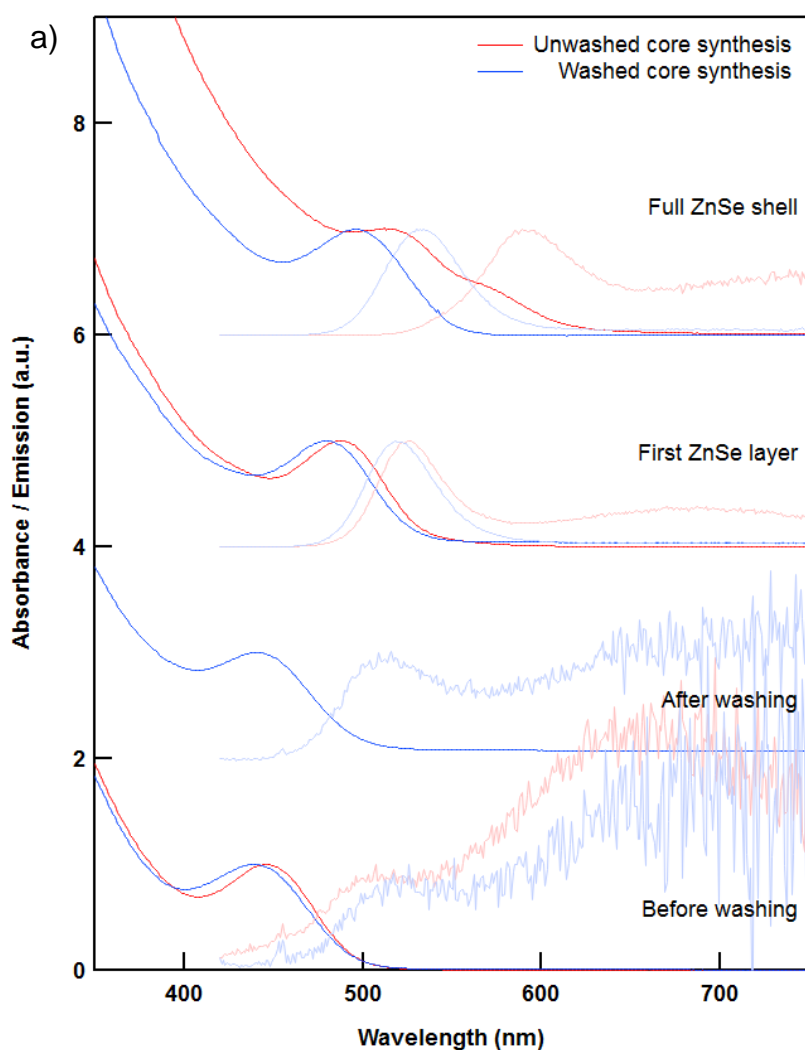


Figure 25. When washing the cores before shell synthesis, the defect emission is lowered significantly. If the cores are not washed before, the absorption (thick lines) and emission (thin lines) broaden and red-shift, as can be seen from the spectroscopic data (a) and from the sample itself (b).

When growing the first, very thin shell layer, the defect emission for especially the clean cores is lowered significantly and there is a visible red-shift. This corresponds to the passivation of the surface (lowering of the low energy emission) and the growth of the particle (red-shift of the absorption and emission peaks). Furthermore, when the first shell layer is not grown perfectly, the defect emission after the first shell layer will remain for the rest of the synthesis (figure 25a.). This is caused by dangling bonds that remain between the core and the shell of the quantum dot.

5.3. Lattice matching with ZnMgSe

As explained in section 2.11., MgSe is the perfect shell material for InZnP quantum dot cores. The crystal structure is however a problem. By attempting the shell synthesis from Ramasamy *et. al.* [51], but by changing the zinc precursor (zinc stearate) partially for magnesium stearate, it was attempted to grow a ZnMgSe shell on previously washed cores.

For the first experiment, one layer of ZnSe was grown during the heating step of the cores in the ODE. This was done, to adjust for the ligands (palmitates on the surface and in the solution) that were lost during the washing step. In this way, the cores cannot be damaged during the heating step. ZnMgSe shell was grown on top of the ZnSe layer. This resulted in quantum dots that broadened slightly with increasing magnesium fractions (figure 26a.). The defect emission increased as well with increasing fractions of magnesium (figure 26b.). The photoluminescence quantum yield (PLQY) seemed to increase for low fractions of magnesium, but then drop rapidly for higher fractions (figure 26c.). To test the stability, the quantum dots were exposed to air. After 48 hours, the samples were remeasured. This showed a decrease in the defect emission for magnesium containing quantum dots, and a stable PLQY for the 100% MgSe sample. The PLQY for the other quantum dots all decreased to about the same level as the MgSe sample. This can be an indication that the MgSe layer was already oxidized during the first measurements, and that after 48 hours, all shell layers were oxidized, hence the PLQY was lowered to the same level.

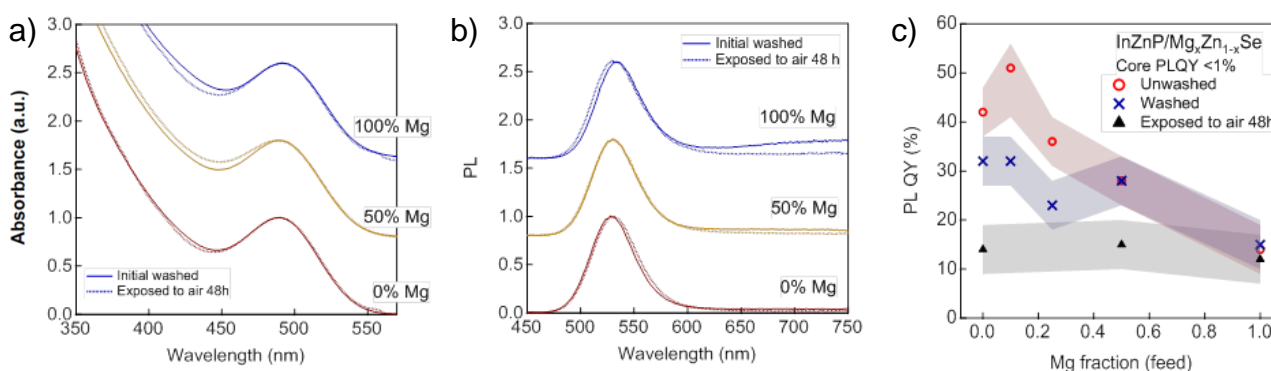


Figure 26. The effects of different fractions of magnesium in the shell material (a). Exposure to air lowers the defect emission significantly (b), but all to similar values (c).

In the experiment of figure 26., first a ZnSe layer was grown on the core to adjust for the loss of ligands and to make the cores more resistant during the heating step. Thereafter, a ZnMgSe shell was grown. If magnesium has beneficial effects, directly growing a ZnMgSe shell on the InZnP cores should improve the degree of surface passivation due to a better lattice match between the core and the shell. To test the effects of directly putting a ZnMgSe shell on the cores, a separate experiment was set up.

The results of this control experiment, displayed in figure 27a., show an increase of defect emission, directly after the addition of the metal precursors (bottom). This increase of defect emission stays after growing the first layer (middle) and the full shell (top). In terms of FWHM, the addition of magnesium is not favorable. Note, exactly the same cores are used for the comparison experiment of figure 27a.

To be able to conclude that this shell synthesis does not improve the optical qualities of the quantum dots, a series of core shell quantum dots was made by the same protocol as before. From figure 27b., it is obvious that, even though the syntheses are unoptimized, the defect emission for every sample is unacceptably high, as well as the fact that all samples have a too large size distribution.

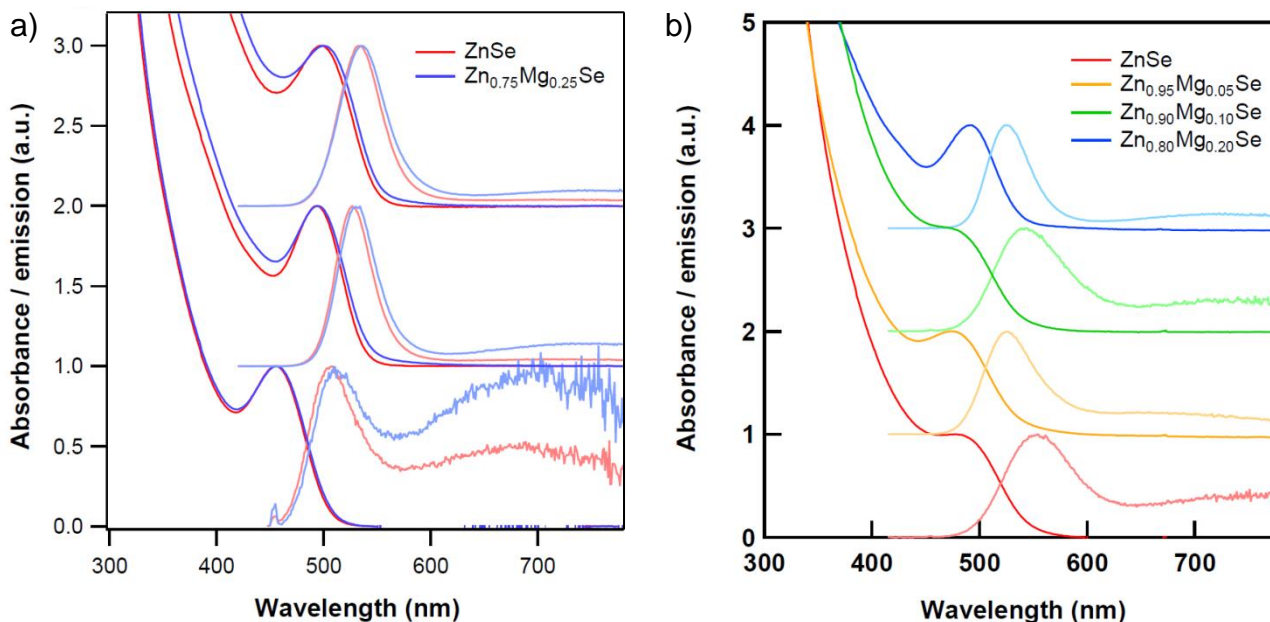


Figure 27. The effects of having a ZnSe layer between the InZnP core and the ZnMgSe shell. It can be seen that the defect emission is lower with the ZnSe layer than with a direct connection between the core and the magnesium containing shell (a). InZnP core quantum dots with ZnMgSe shells with different fractions of magnesium in it show a large size distribution and significant defect emission (b).

5.4. Shell study required

As can be seen from the results in this chapter, the cores should be washed in order to get good quality core – shell quantum dots (5.1.). The growth of a shell greatly increases the PLQY of the quantum dots (5.2.). When incorporating magnesium in the shell, the expected increase due to better lattice matching is translated to a decrease of PLQY for the experimental results (5.3.). First passivating the core with a ZnSe layer is beneficial, but counterintuitive, because the ZnMgSe material should match the core (hence passivate the surface) better. Therefore, it was decided to study the ZnMgSe material. The aim of this study is to test if ZnMgSe is synthesized under the conditions just described to grow shells of ZnMgSe. If ZnMgSe is synthesized, the aim is further to determine what the lattice parameter of this material is. This will help to understand the competing effects of beneficial lattice matching, versus the detrimental hygroscopicity and oxophilicity of zinc magnesium selenide.

6. ZnMgSe nanoparticle synthesis

As explained in the previous chapter, the aim is to study pure ZnMgSe with various magnesium fractions, to see if the material is synthesized and what the lattice parameters of the material with different fractions of magnesium is. To be able to easily study the shell material, nanoparticles of the shell material were made (6.1.). The materials formed were studied with TEM, electron diffraction (ED) and EDX. ED was chosen over XRD, because ED could be performed in the TEM, therefore the water and oxygen sensitive samples did not have to be exposed to air (for a long time). These characterizations were performed to prove that first of all the lattice constant of the ZnMgSe does match better with the InZnP quantum dot core and secondly, the crystal structure is a zinc blende so that also matches with the InZnP core. In section 6.2., the results obtained are evaluated and from there, the following synthesis steps were determined.

6.1. ZnMgSe synthesis with metal stearates and TBP-Se

The synthesis method of ZnMgSe nanoparticles is based on a research article from Li *et al.* [52] The procedure is developed for the synthesis of pure ZnSe nanoparticles, but it uses TBP-Se instead of TOP-Se, which was used in the shell syntheses of section 5.2. The reaction is furthermore carried out in a different solvent. By the addition of magnesium stearate, it was attempted to synthesize ZnMgSe. This synthesis gave better results than the syntheses using TOP-Se at lower temperature (6.1.), as can be seen in figure 28a. The peaks between 300 nm and 350 nm are related to the metal precursors. The peaks at 371 nm and 398 nm for the ZnMgSe and the ZnSe respectively, correspond to formed nanoparticles. For the MgSe, no low energy peak is observed, which means pure MgSe is probably not grown with this synthesis.

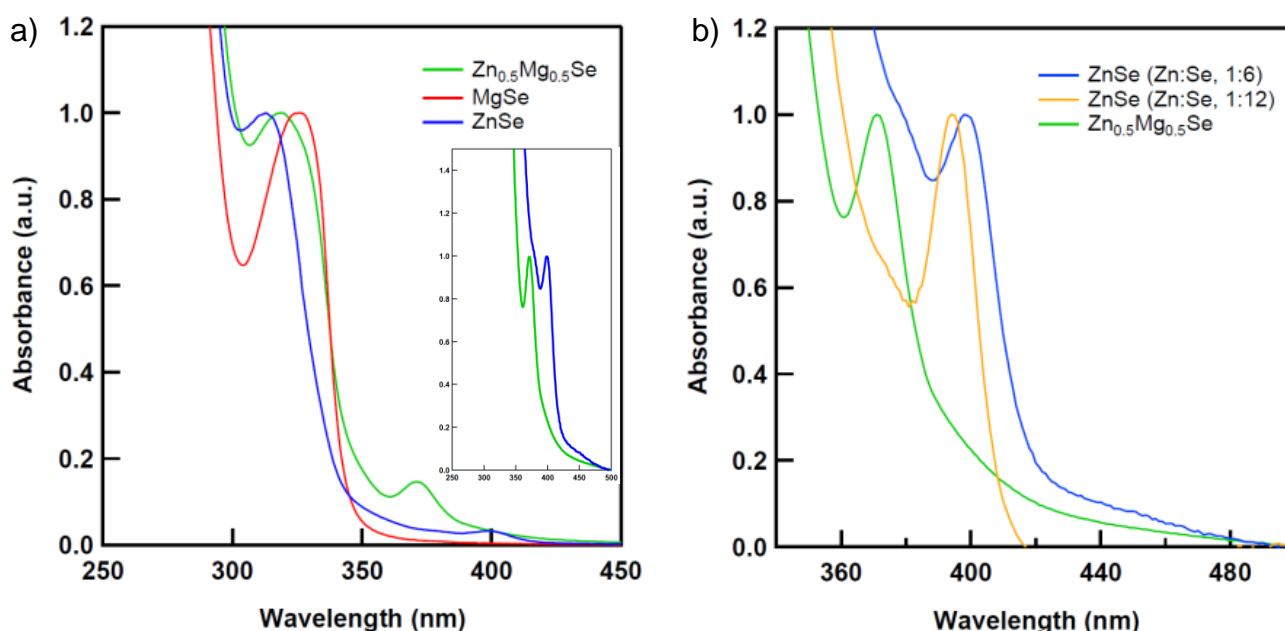


Figure 28. Absorption spectra of ZnSe, ZnMgSe and MgSe synthesized by the method of Li *et al.* [51] The peaks at 371 nm and 398 nm for the ZnMgSe and the ZnSe respectively, correspond to formed nanoparticles (a). The blue-shift for the ZnMgSe does not seem to be caused by the different Zn:Se ratio, because the absorbance for the two ZnSe materials, synthesized with different Zn:Se ratios, have a maximum around the same point (b).

From figure 28a. it is obvious that, when including magnesium stearate in the reaction mixture, the absorbance blue-shifts with increasing concentrations of magnesium. To show that this blue-shift is directly related to the presence of magnesium, and not due to the lower Zn:Se ratio, a control experiment was performed where the same Zn:Se ratio was used. The results, shown in figure 28b., directly indicate that the blue-shift is not due to the changed Zn:Se ratio. However, it can still be that by having magnesium stearate in the reaction mixture, the reaction kinetics are changed where the magnesium stearate acts as a growth limiting ligand.

For the synthesis of figures 28a. and 28b., a mixture of ODE and tetracosane is used as the solvent, which is solid mixture at room temperature. To make the nanoparticles retrievable, just like the synthesis from 6.1., the synthesis was performed in pure ODE. The results, shown in figure 29a., do not show a big difference from the tetracosane containing syntheses. Therefore, the particles from these syntheses were studied with TEM and electron diffraction (figure 29b.). From the data that was obtained from these characterization methods (ED data was converted to radial intensity, using CrystBox software), it was concluded that for this synthesis, as well as for the synthesis from 6.1., mostly metal stearates were measured, rather than monodisperse Zn(Mg)Se nanoparticles. Furthermore, the signals that were found in the electron diffraction belonged to ZnSe, rather than ZnMgSe. This was concluded, because no shift in the radius of the radial profile was found. This means that there is no lattice expansion, which is expected for ZnMgSe.

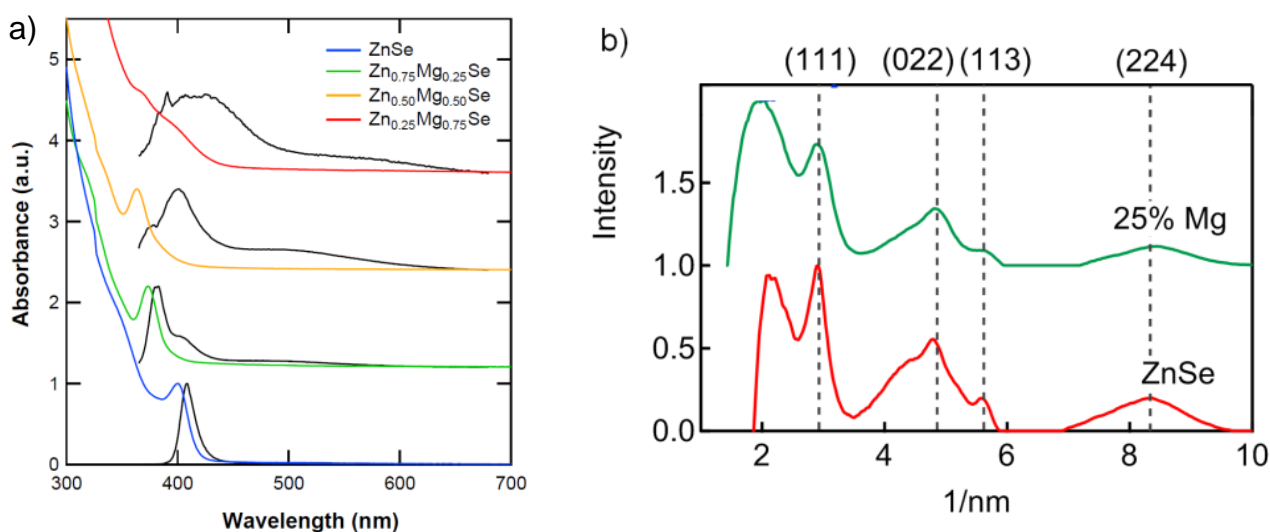


Figure 29. Zn(Mg)Se with different fractions of magnesium show a blue-shift in the absorption. The photoluminescence of these samples only partially follows this trend (black lines, (a)). Electron diffraction patterns show no difference between the lattice parameters of ZnSe and ZnMgSe (b).

6.2. More reactive precursors

ZnMgSe nanoparticle synthesis with the same precursors as used for the shell growth in section 5.3. did not seem to work (6.1.). Therefore it can be concluded that the shells grown in section 5.3. are not of a good quality. Thereafter, a synthesis method using a more reactive selenium precursor was tried at a higher temperature. Even though ED showed that particles formed, there was no evidence of the incorporation of magnesium, because the lattice did not expand. To make sure that both metals are incorporated in the nanoparticles, it was decided to try syntheses using much more reactive, organometallic precursors. These syntheses will be treated in chapter 7.

7. ZnMgSe synthesis using organometallics

From chapter 6. it seemed that the reactivity of the metal stearates towards the selenium precursor is a problem. Therefore, much more reactive organometallic precursors were tried. The synthesis was performed according to the research article from Boldt *et al.* [53] In this article, ZnSe nanoparticles are formed using diethylzinc. For the magnesium precursor, dibutylmagnesium was chosen.

7.1. Combined metal precursor synthesis

In the synthetic procedure of Boldt *et al.* the selenium precursor (TOP-Se) and the diethylzinc are combined together into a syringe, and quickly injected in oleylamine (OLA) at 300°C. When the dibutylmagnesium is added to the injection solution, a white precipitate forms directly, indicating the dibutylmagnesium already reacts before injection. Therefore, the metal precursors were combined in one syringe, and added quickly after the injection of the TOP-Se. This synthesis method gave very distinct features for both the ZnSe as the ZnMgSe synthesis. The most obvious difference between this synthesis and the syntheses using metal stearates (chapter 6.), is a red-shift for the magnesium containing product, rather than a blue-shift (figure 30a.).

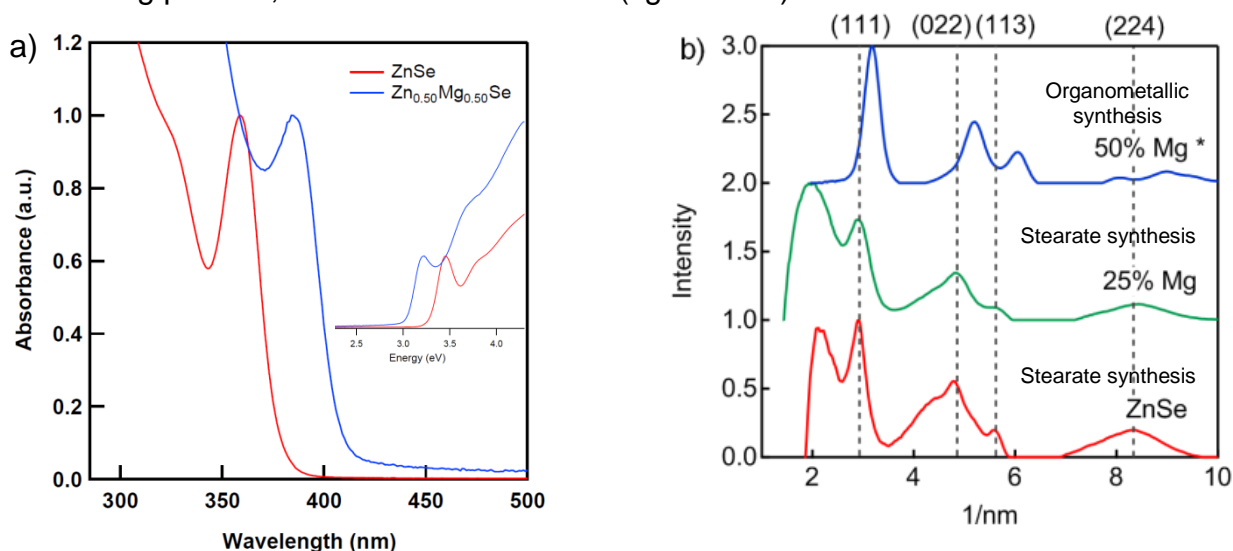


Figure 30. The absorption spectra (a) of the ZnSe and ZnMgSe made by the method of Boldt *et al.* [52] clearly show a red-shift for the magnesium containing material compared to the pure ZnSe. Furthermore, the electron diffraction data of the ZnMgSe (b), shows a clear difference in the intensity of the signals, as well as a shift of the peaks for the organometallic synthesis, compared to the stearate syntheses of section 6.1.

Electron diffraction (figure 30b.) indicated that the lattice parameters from the ZnSe (black lines) differed from the $Zn_{0.50}Mg_{0.50}Se$ (green spectrum). The $Zn_{0.50}Mg_{0.50}Se$ however, showed a lattice contraction compared to the ZnSe samples (shift to the right), instead of a lattice expansion that is preferred for the better lattice match on the InZnP quantum dot cores. Note that the comparison is made with ZnSe synthesized by using stearates.

Altogether, this synthesis seems to conclude that ZnMgSe is synthesized, but that there is a lattice contraction, rather than a lattice expansion. This contraction can be caused by the formation of other materials (zinc magnesium selenates or oxides) or by ZnMgSe in the wrong, rock salt crystal structure. Therefore, the experiments indicate that this material is not beneficial to grow around the InZnP cores.

7.2. MgSe synthesis for crystallography

To be able to conclude that there was a change of the crystal structure, ZnSe, ZnMgSe and MgSe were synthesized by the same method, using organometallic precursors. The MgSe nanoparticles were not retrievable and showed a broad emission (figure 31a.). However the ZnMgSe was blue-shifted compared to the ZnSe sample, indicating a wider bandgap material which could improve the properties of the InZnP quantum dots. To see what happened, absorption spectra of washed and unwashed samples were compared (figure 31b.). This showed that the sample of figure 30a. was blue-shifted a lot after washing. This is most probably related to the aggressive washing that etched away the surface of the nanoparticle, and thereby making the nanoparticle smaller. As said before, smaller particles have emission of a higher energy, hence the aggressiveness of the washing, or rather the difference in aggressiveness between the wash of the ZnSe and the ZnMgSe of the sample of section 7.1. could explain the red-shifted ZnMgSe absorption.

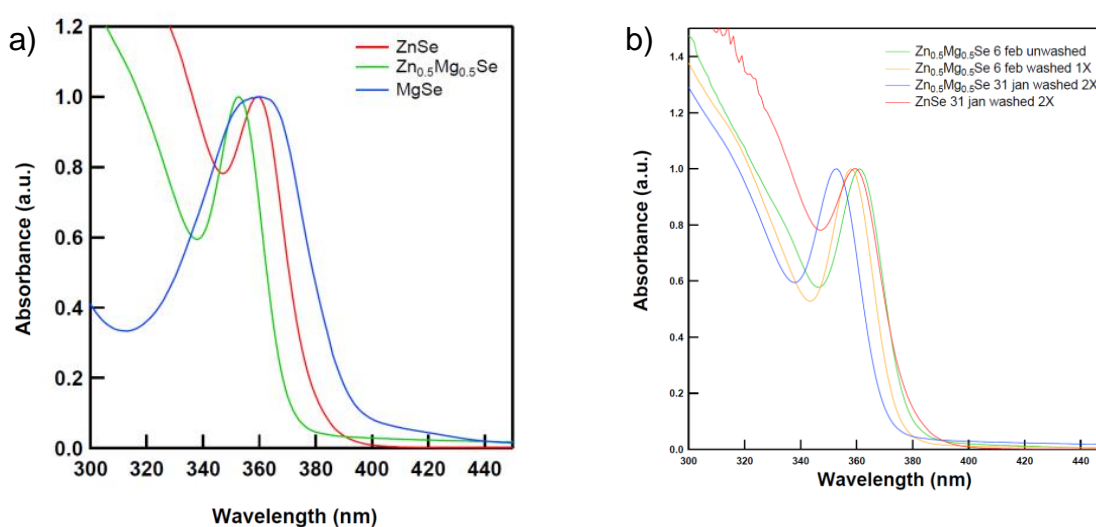


Figure 31. The absorption of MgSe shows a broadening, whereas ZnSe and ZnMgSe show narrow peaks (a). Most notable is the blue-shift for ZnMgSe compared to ZnSe, which is in contrast to the results obtained before. Washing of the samples seems to affect the absorption wavelength drastically due to etching of the surface (b).

TEM images showed smaller particles for the magnesium containing sample (figure 32b.) compared to ZnSe particles (figure 32a.), which formed bigger structures (potentially gels of zinc magnesium selenite or oxide), as can be seen in figure 32c. To be sure whether ZnMgSe is blue-shifted or red-shifted compared to ZnSe, it was decided to grow a protective ZnS shell around the Zn(Mg)Se nanoparticle, to stop etching of the nanoparticle surface, and furthermore to protect it from any possible oxidation or hydrolysis.

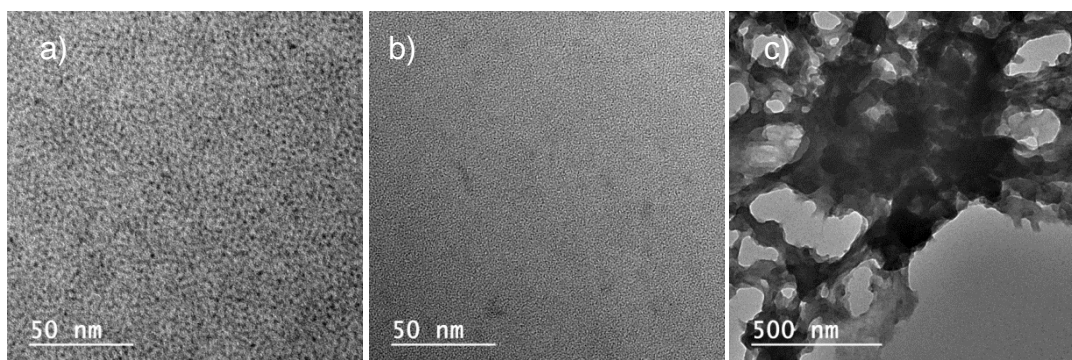


Figure 32. TEM images of ZnSe (a) and ZnMgSe with 50% Mg (b). The ZnMgSe formed big structures that contained the smaller particles (c).

7.3. ZnS protected ZnMgSe synthesis

As explained in section 7.2., etching of the surface might influence the results obtained so much, that the actual absorption of ZnMgSe can be both blue-shifted or red-shifted. Therefore, a zinc sulfide shell was grown on the Zn(Mg)Se nanoparticles after the synthesis was completed, by the subsequent addition of more diethylzinc and TOP-S (the sulfur containing analog of TOP-Se).

The syntheses of ZnSe and $\text{Zn}_{0.50}\text{Mg}_{0.50}\text{Se}$ were performed exactly as the syntheses in sections 7.1. and 7.2. However, when combining the diethylzinc and dibutylmagnesium together for samples with 10% and 25% of magnesium, the organometallic precursors directly became turbid and a white precipitate was formed immediately. This indicated that the two metal precursors, when combined, also prereact, just as for the combination of dibutylmagnesium and TOP-Se (section 7.1.). Probably the 50% magnesium containing metal precursor solution formed a soluble reaction product. For the 10% and 25% of magnesium containing samples, it was chosen to inject the metal precursors at the same time, but from two different syringes. The results of the four syntheses, shown in figure 33a., show a clear blue-shift for the 10% and the 25% magnesium containing samples compared to ZnSe. The 50% magnesium containing sample shows a red-shift. This sample however was made with the metal precursors mixed together. All samples show the same emission characteristics in terms of color and brightness (figure 33b.).

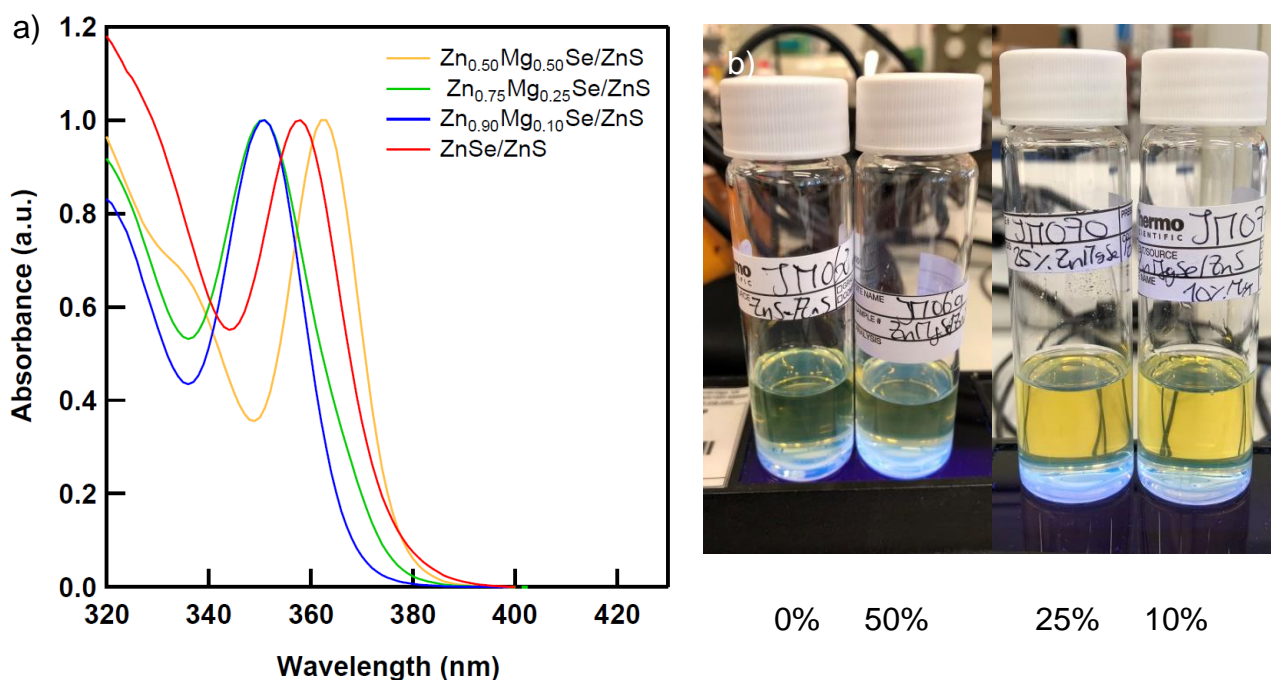


Figure 33. The absorption of ZnSe and ZnMgSe with various fractions of magnesium (a) and the emission, visible from the samples (b).

Electron diffraction showed that the 0%, 25% and 50% magnesium containing samples all have the same crystal structure. This can be concluded, because the shapes and relative intensities are the same for all diffraction patterns (figure 34.).

Furthermore, this figure shows that there is a slight shift of the peaks, most visible for the (111) plane. With increasing fractions of magnesium, the peak shifts to lower 1/r-values, indicating a lattice expansion. In table 7., the relative expansion is shown. Because the lattice mismatch between InZnP and ZnSe is caused by a too low lattice constant of the ZnSe shell material, a lattice expansion is preferred. TEM furthermore showed that the particles formed were spherical nanoparticles. EDX indicated that magnesium is incorporated in the material, however in a lower fraction than added to the reaction.

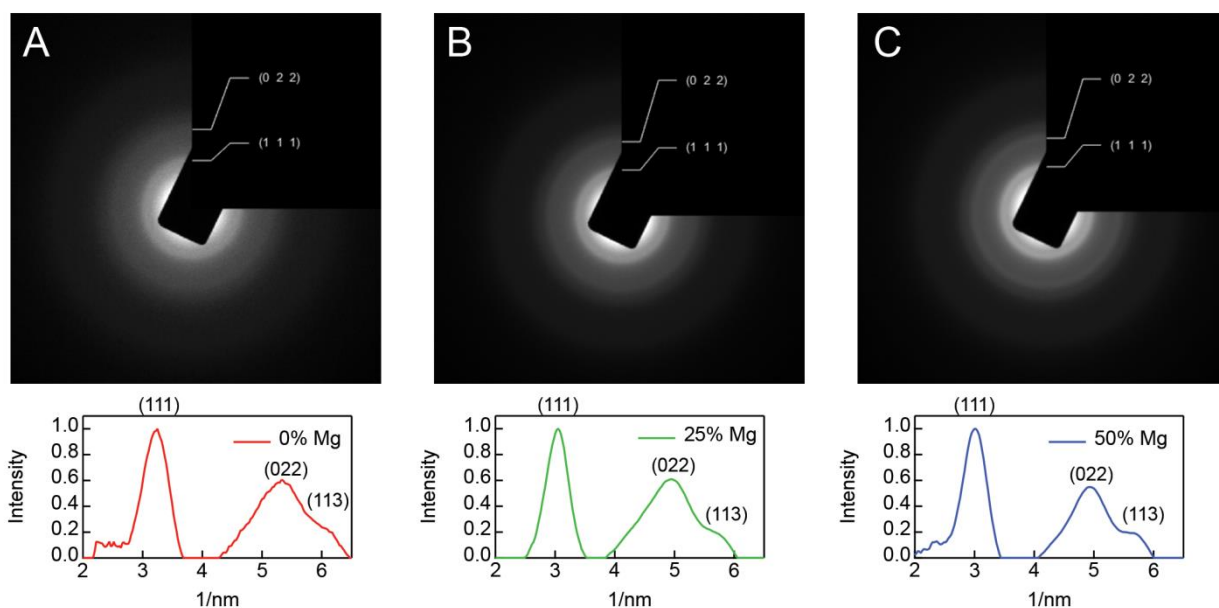


Figure 34. Electron diffraction patterns (radial profiles and transformed data) for different fractions of magnesium in the ZnMgSe nanoparticles (0% (a), 25% (b) and 50% (c)).

Table 7. Increased lattice spacing for ZnSe alloyed with magnesium

Sample	(111) d-spacing	(111) lattice change vs ZnSe/ZnS	(022) d-spacing	(022) lattice change vs ZnSe/ZnS
0% Mg	0.310 nm	-	0.188 nm	-
25% Mg	0.328 nm	+ 5.8%	0.202 nm	+ 7.4%
50% Mg	0.333 nm	+ 7.4%	0.203 nm	+ 7.9%

7.4. Chosen shell growth methods

Magnesium containing shell growth syntheses did not show to work with stearate precursors (chapter 6.). Organometallic precursors do form material with different absorption peaks (7.1.), but washing can influence the results by etching of the surface (7.2.). Therefore the material should be protected by a thick ZnS layer (7.3.). Also, the metal precursors need to be added separately, because the dibutylmagnesium prereacts with both the TOP-Se (7.1.) as the diethylzinc (7.3.).

In the end it was shown that the lattice of ZnSe expands when magnesium is incorporated. Therefore, this material seems to be promising as an improved shell material compared to ZnSe.

8. InZnP/ZnMgSe synthesis using organometallics

It was confirmed that ZnMgSe can be grown using organometallic precursors (chapter 7.). Therefore, it was attempted to grow a ZnMgSe shell around InZnP cores. The synthesis was done using the same method as used in the article of Ramasamy et al. [51], but the metal stearate precursors were changed to organometallic precursors.

The absorption and emission spectra (figure 35a.) of these batches show a broader size distribution than for the previous syntheses. The FWHM of the quantum dots with a 20% fraction of magnesium in the shell have a narrower FWHM than the once with a ZnSe shell. There is relatively much defect emission, but this is about the same for the ZnSe as for the ZnMgSe shell. This is caused by a far from optimized protocol for this synthesis. Another possible reason is an aluminium impurity which is added on purpose to the dibutylmagnesium (1%, as triethylaluminium) as a viscosity reducer.

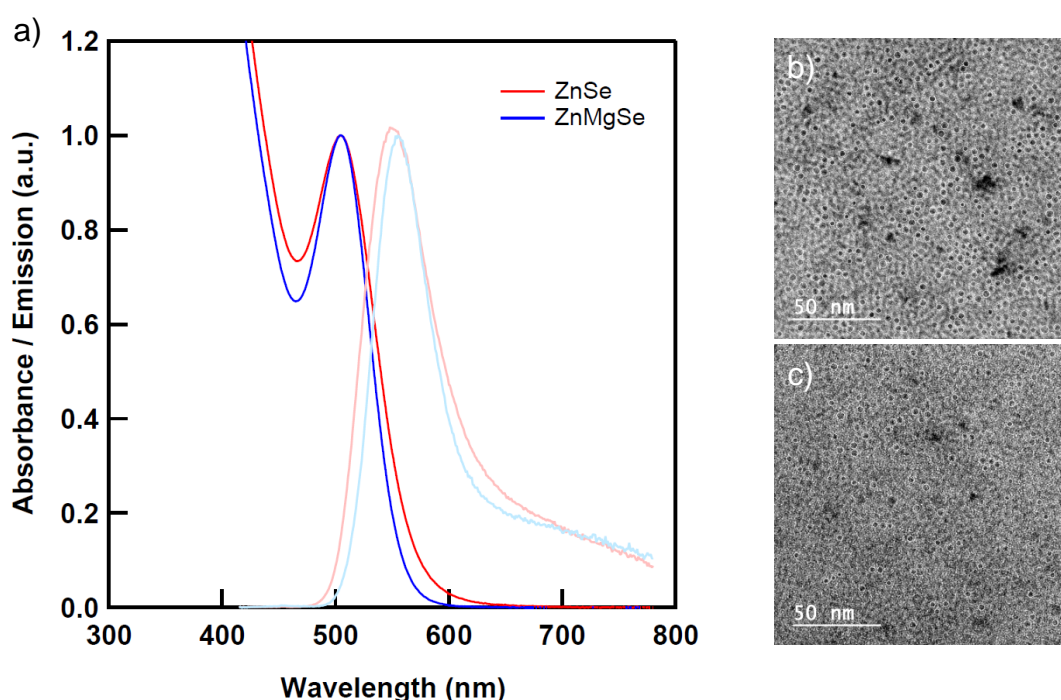


Figure 35. A difference in absorption and emission can be seen for QDs with ZnSe and ZnMgSe shells, where magnesium seems to have a positive influence on the FWHM of both peaks (a). TEM images do not show a clear difference between the size or appearance of the two batches (ZnSe (b) and ZnMgSe (c)).

TEM imaging showed quantum dots that were determined to have around the same size. The size of the QDs with a ZnSe shell was 3.638 ± 0.529 nm (figure 35b.). The size of the QDs with a ZnMgSe shell was 3.504 ± 0.448 nm (figure 35c.).

Because the ZnMgSe layer is not stable in air, it was decided to protect the quantum dots with a protective second ZnS shell layer. Furthermore, it was decided to grow the Zn(Mg)Se shell layer in a more controlled way, at a lower temperature. This, because the broadening of the emission spectra might have been caused by the use of too reactive chemicals, where the Zn(Mg)Se was grown randomly, rather than controlled. A solution might be the use of Grignard reagents like butylmagnesium chloride, which is less reactive than dibutylmagnesium, but more reactive than magnesium stearate.

9. InZnP/ZnMgSe/ZnS core-shell-shell synthesis

In this chapter, the results from chapters 4 to 8 are combined, in order to synthesize the best InZnP/ZnMgSe/ZnS core – shell – shell quantum dots. Before treating quantum dots with shells made by using organometallic precursors, first the influence of a ZnS shell on InZnP/ZnSe core – shell quantum dots is evaluated (9.1.). Subsequently, the effects of magnesium in the shell are discussed. This leads to the final conclusion about the use of magnesium to improve the PLQY, stability and color purity of the quantum dots (chapter 10.).

9.1. ZnS shell synthesis on InZnP/ZnMgSe QDs

To determine the effects of a ZnS layer on the core – shell quantum dots, a batch of quantum dots was made according to the synthesis by Ramasamy *et al.* [51] This synthesis is using stearate precursors and TOP-Se for the ZnSe shell. Magnesium stearate was added, to make a ZnMgSe shell. As explained in chapter 6., the magnesium probably is not incorporated in this shell. The other difference with the synthesis described in the article, is a change for the precursors of the ZnS shell. The precursors used are zinc stearate and TOP-S, instead of zinc oleate and 1-dodecanethiol

From the results, shown in figure 36a., the most notable is a red-shift of the absorption and emission. This can also be seen in the emission of the samples (figure 36b.). The red-shift is caused by the increased size of the quantum dots. The ZnS shell seems to have a high enough bandgap to have a pure type I band alignment, because there is no red-shift or broadening of the FWHM, hence there is no delocalization of the excited hole or the electron.

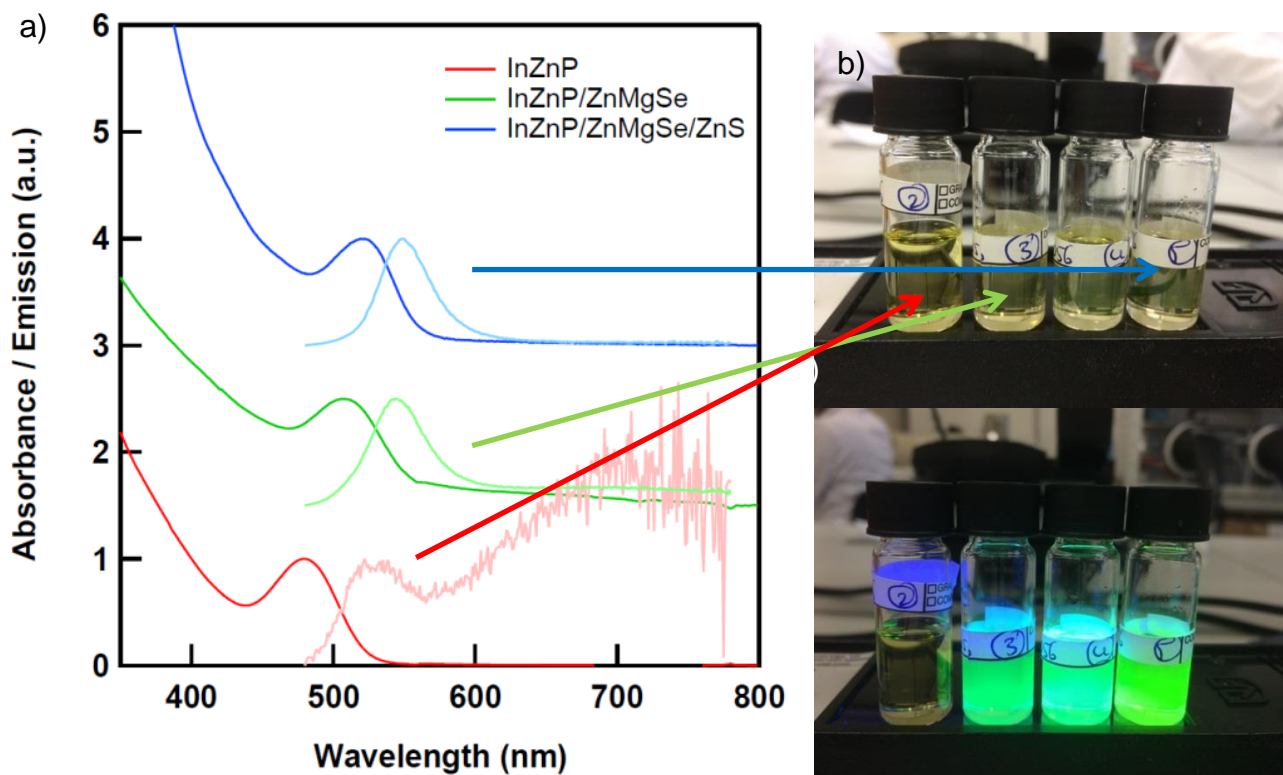


Figure 36. The effects of an additional ZnS shell around InZnP/ZnMgSe core shell quantum dots. There is a clear red-shift in the emission spectrum (a), which is more clearly seen from the samples themselves (b).

9.2. The beneficial effects of ZnMgSe over ZnSe

The main issue with current indium phosphide quantum dots is the lattice mismatch between the core and the shell material (section 2.11.). After determining the core synthesis method to obtain the quantum dots with the highest color purity *i.e.* lowest FWHM (section 4.3.) and the best ZnMgSe shell synthesis method (section 7.4.), the aim of the research in this section is to combine the core and shell, to determine if there is an improvement between the lattice match of the core and the shell material when incorporating magnesium in the shell material.

The results of the syntheses, explained in section 3.8., are far from perfect, because this synthesis is not optimized in any way. Estimations have been made for the solvent to use, the optimal fraction of magnesium, the temperature of the ZnMgSe and ZnS shell growth reactions, as well as the optimal thickness of both shell layers.

The solvent chosen is a 1:1 mixture of octadecene (ODE) and oleylamine (OLA), because ODE is generally used as the solvent for these syntheses when using carboxylate precursors. OLA was added, because the quantum dot cores did not have many ligands on their surface after the washing step. Heating the cores in pure ODE would damage the cores. Furthermore, it was chosen to compare a ZnSe shell which is currently used to a ZnMgSe with a fraction of 50% magnesium as this was calculated to have the best lattice match (section 2.11.). The shell growth temperatures were set to 200°C for the ZnMgSe shell and 240°C for the ZnS shell, as this temperature range is more frequently used for the growth of shells with organometallic precursors. The ZnS shell synthesis was chosen to have a slightly increased temperature, to be able to anneal any defects created. The shell thickness for the ZnMgSe shell was kept the same as for the synthesis described in the article of Ramasamy *et al.* [51] The ZnS shell growth, and influence of the thickness of the ZnS shell layer on the InZnP/ZnMgSe quantum dots was monitored by taking aliquots after each addition of ZnS precursor solution (figure 37.).

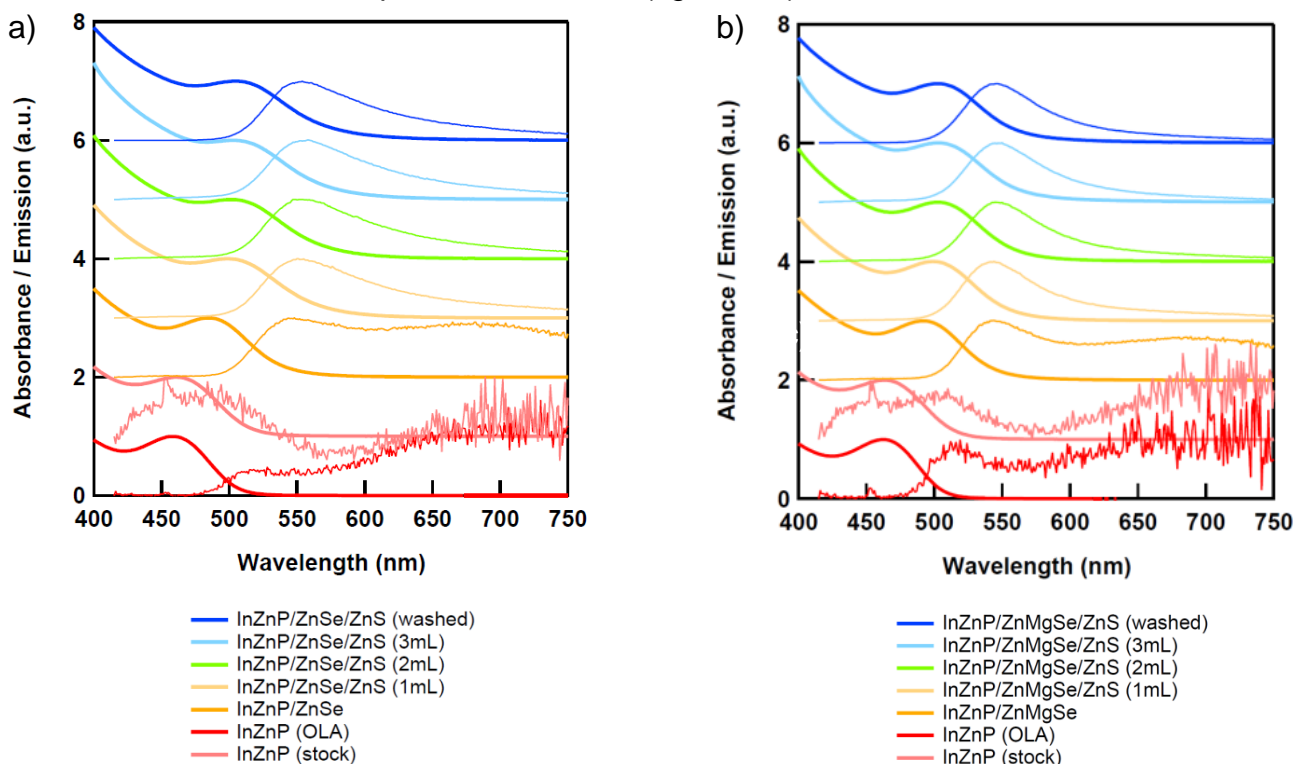


Figure 37. Absorbance and emission spectra of quantum dots without (a) and with (b) magnesium in the shell material.

From figure 37., it can be seen that the samples with a ZnSe shell, have a large fraction of lower energy emission. For the ZnMgSe shell, this can also be seen, however it is substantially lower. Note that there is no difference in the cores, because the same batch of cores was used for both syntheses. In figure 38a., the quantum dots with a ZnSe and a ZnMgSe are compared. On the bottom of this graph, the core-shell quantum dots without ZnS layer are depicted, showing a lower fraction of lower energy emission for the magnesium containing shell layer. After the first milliliter of ZnS precursor solution added, the differences increase, showing a much narrower absorption and emission for the magnesium containing shell (middle of the graph). This effect stays after the full shell was grown (3.2 mL of precursor solution) and the sample was washed (top of the graph).

The results observed from figure 38a. are also visible from the samples (figure 38 b,c.). The emission from the samples with a ZnSe shell appear yellow due to the broadening of the emission spectrum. The emission of the samples with a ZnMgSe shell appears green, because the emission peak is much narrower. The calculated FWHM and HWHM of all aliquots, shown in table 8., indicate that the difference in broadness is made during the growth of the Zn(Mg)Se layer, at the point where the lattice match should be improved.

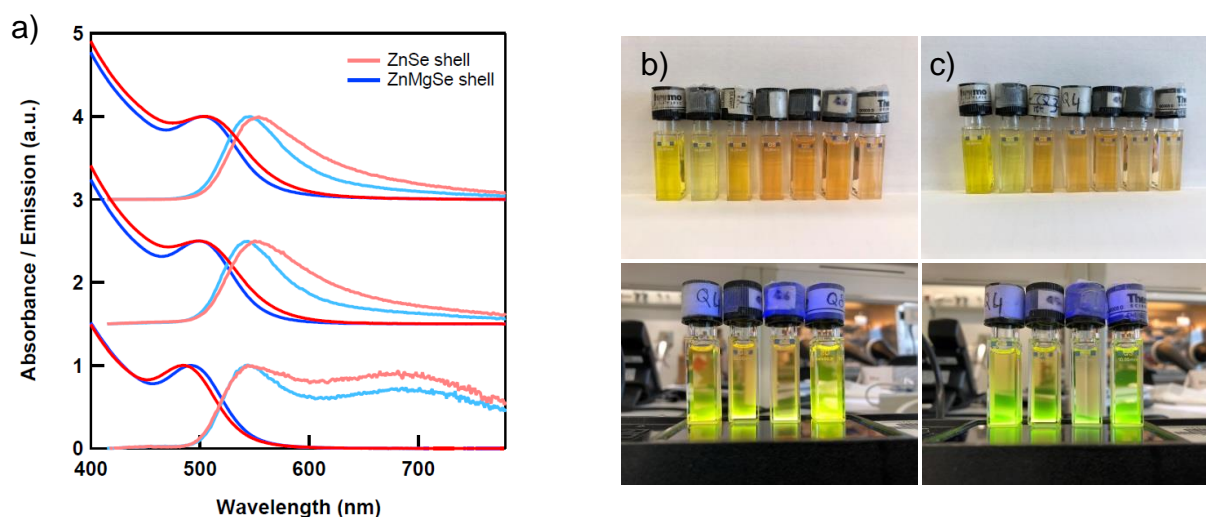


Figure 38. Comparison of absorbance and emission spectra of quantum dots with and without magnesium in the shell material (a) for the InZnP/Zn(Mg)Se QDs (bottom), after 1 mL of ZnS precursor addition (middle) and the final QDs (top). A clear red-shift for the emission is seen for the QDs with a ZnSe shell (b) compared to those with a ZnMgSe.

Table 8. Color purity of the InZnP QDs with a ZnSe and a ZnMgSe shell.

Stage	ZnSe shell		ZnMgSe shell	
	HWHM absorbance (nm)	FWHM emission (nm)	HWHM absorbance (nm)	FWHM emission (nm)
InZnP (stock)	30	44	28	46
InZnP (OLA)	33	– ¹	32	– ¹
InZnP/Zn(Mg)Se	35	62	32	52
InZnP/Zn(Mg)Se/ZnS (1mL)	43	96	34	66
InZnP/Zn(Mg)Se/ZnS (1mL)	45	95	36	68
InZnP/Zn(Mg)Se/ZnS (1mL)	46	93	38	68
InZnP/Zn(Mg)Se/ZnS (washed)	43	91	37	68

¹ Due to the emission from oleylamine, the FWHM of the emission peak of the cores is not determinable.

PLQY calculations, using an integrating sphere, showed a PLQY of 6.0% for the quantum dots with a ZnSe shell, and a PLQY of 7.5% with a ZnMgSe shell. The absolute PLQY is very low for both samples, because the synthesis is far from optimized. The relative improvement for the quantum dots with a magnesium containing shell is however 25%.

The growth of the ZnS shell should have been stopped earlier, as can be seen from the intensity of the emission. This decreases after the addition of every extra milliliter (figure 39.).

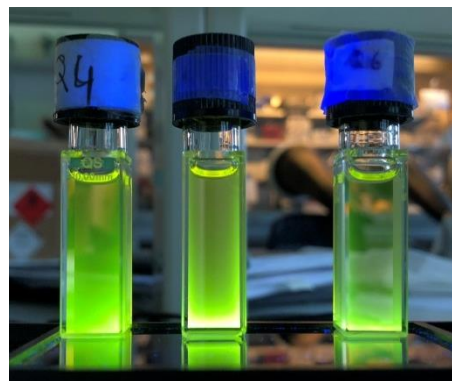


Figure 39. A decrease of emission intensity is seen after each addition of ZnS precursor, due to the growth of a too thick ZnS shell.

10. Conclusions

To remove cadmium based quantum dots from commercial applications, InZnP is a good alternative. To improve the stability of the InZnP core quantum dot, an inorganic, epitaxially grown shell is determined to be the best option, to entirely isolate the quantum dot core from the exterior, thereby protecting it from oxygen and moisture from the air. The color purity, measured in terms of FWHM, is best for the heating up synthesis.

In order to have a high PLQY, there needs to be a good match between the core and the shell, to remove dangling bonds. This can only be done after removing all excess reactants by washing freshly prepared cores, before the shell synthesis is performed, otherwise the absorption and emission bands broaden. Incorporating magnesium in the shell increases the PLQY and the color purity. After the ZnMgSe shell is synthesized, a ZnS shell is needed as second shell, to protect the ZnMgSe material itself from hydrolysis and oxidation.

Furthermore, it is possible to synthesize blue emitting ZnMgSe nanoparticles with a very narrow FWHM. The emission peak depends on the fraction of magnesium incorporated in the material, where an increased fraction of magnesium leads to a blue-shift.

10.1. Future research

Next to improving the lattice match between InZnP quantum dot cores and the shell by making a ZnMgSe shell, there are more possibilities that can be added or changed to the quantum dots.

First of all, a gallium cation exchange on the quantum dot cores can be added to the synthesis of the quantum dots synthesized in section 8.2. For the hot injection synthesis, a gallium cation exchange proved to increase the PLQY. [50]

Secondly, a graded shell composition, where the amount of magnesium is lowered for every next shell layer can help to reduce the amount of strain in the shell material. This might optimize the shell structure, especially for thicker shells. Also, it would improve the lattice match between the Zn(Mg)Se layer and the ZnS layer.

Next to this, a magnesium for zinc cation exchange can be an option for incorporating magnesium in the shell. If incorporation of magnesium indeed leads to an improved lattice match, it would be thermodynamically favorable to exchange magnesium for zinc, which, when incorporated would diffuse towards the core – shell interface, where it would fit best. When choosing the correct ligands, zinc might be taken out and exchanged for magnesium.

Also, when the organometallic precursors used are too reactive, it can be tried to use reactants that have a reactivity between that of the organometallic precursors used and the stearates. Grignard reagents, organometallic compounds where one of the two ligands is substituted by a halide ion, might be a good option.

The influence of impurities in the reactants cannot be excluded. One of the major impurities to take into account is an aluminium impurity. The dibutylmagnesium contains up to 1% triethylaluminium as a viscosity reducer. This however can significantly influence the lattice match between the core and the shell, which is most important to reduce the recombination in trap states.

At last, instead of changing the cation, changing the anion of the shell layer can also be an option. When making a ZnTeSe material, the lattice match should be perfect around 50% tellurium. The band alignment might be a problem when incorporating too much tellurium (because it changes from a type I to a type II material).

Bibliography

1. Svitkova, V., et al., *Assessment of CdS quantum dots effect on UV damage to DNA using a DNA/quantum dots structured electrochemical biosensor and DNA biosensing in solution*. Sensors and Actuators B: Chemical, 2017. **243**: p. 435-444.
2. Machol, J.L., et al., *Optical studies of IV0VI quantum dots*. Physica A, 1994. **207**: p. 427-434.
3. Assareh Pour, F. and H. Zandi, *DFT electron transport study of quantum dot sensitized solar cells linkers*. Optik - International Journal for Light and Electron Optics, 2017. **143**: p. 199-204.
4. Borah, P., et al., *Quantum confinement induced shift in energy band edges and band gap of a spherical quantum dot*. Physica B: Condensed Matter, 2017(Accepted manuscript).
5. Karwacki, Ł., *Magnon cotunneling through a quantum dot*. Journal of Magnetism and Magnetic Materials, 2017. **441**: p. 764-768.
6. Cao, S. and X. An, *White light emitting ternary quantum dots phosphors with controllable chromaticity and fluorescence resonance energy transfer*. Materials Letters, 2015. **155**: p. 118-120.
7. Omata, T., et al., *Quantum dot phosphors and their application to inorganic electroluminescence device*. Thin Solid Films, 2012. **520**(10): p. 3829-3834.
8. Sorokin, S.V., et al., *CdTe/Zn(Mg)(Se)Te quantum dots for single photon emitters grown by MBE*. Journal of Crystal Growth, 2017. **477**: p. 127-130.
9. Yue, P.Y., et al., *Single photon emissions from InAs/GaAs quantum dots embedded in GaAs/SiO₂ hybrid microdisks*. Optics Communications, 2018. **411**: p. 114-118.
10. Dey, S.C. and S.S. Nath, *Electroluminescence of colloidal ZnSe quantum dots*. Journal of Luminescence, 2011. **131**(12): p. 2707-2710.
11. Lenkeviciute, B., et al., *Hybrid OLEDs with CdSSe_{1-x}/ZnS core-shell quantum dots: An investigation of electroluminescence properties*. Synthetic Metals, 2015. **209**: p. 343-347.
12. Arya, H., et al., *Quantum dots in bio-imaging: Revolution by the small*. Biochem Biophys Res Commun, 2005. **329**(4): p. 1173-1177.
13. Martinić, I., S.V. Eliseeva, and S. Petoud, *Near-infrared emitting probes for biological imaging: Organic fluorophores, quantum dots, fluorescent proteins, lanthanide(III) complexes and nanomaterials*. Journal of Luminescence, 2017. **189**: p. 19-43.
14. Meiners, A., et al., *Conjugation of spin labeled proteins to fluorescent quantum dots**. Materials Today: Proceedings, 2017. **4**: p. S180-S187.
15. J.S. Steckel, H. Yamamoto, and P.S. Drzaic, *Quantum dot spacing for high efficiency quantum dot led displays*, in US20170271605 A1. 2017.
16. E.H. Sargent, et al., *Quantum dot optical devices with enhanced gain and sensitivity and methods of making same*, in US 20140291608 A1. 2014.
17. S.J. Liu, H.Y.A. Fong, and Y.T. Lan, *Patent Portfolio Deployment*. 2017: World Scientific. ISBN 9789813142459, p. 189.
18. SONY. *Trademarks and copyright*. 2017; Available from: <https://www.sonymobile.com/gb/legal/trademarks-and-copyright/>.
19. Larsen, R. *Sony Triluminos in W900 uses Quantum Dots*. 2013; Available from: <https://www.flatpanelshd.com/news.php?subaction=showfull&id=1358342209>.
20. Shimizu, K.T., et al., *Toward commercial realization of quantum dot based white light-emitting diodes for general illumination*. Photonics Research, 2017. **5**(2): p. A1.

21. Samsung. *QE65Q7F 65" Q7F Smart 4K Ultra HD HDR QLED TV*. 2017; Available from: <https://www.simplyelectricals.co.uk/euronics-samsung-qe65q7f-65-q7f-class-hdr-qled-4k-tv>.
22. Lennihan, M., *Quantum Dots Make LED Lightbulbs Emit More Pleasant Light*. 2009.
23. Dong, S.-C., L. Xu, and C.W. Tang, *Chemical degradation mechanism of TAPC as hole transport layer in blue phosphorescent OLED*. *Organic Electronics*, 2017. **42**: p. 379-386.
24. Pandey, R., et al., *Strong luminescence behavior of mono- and dimeric imidazoquinazolines: Swift OLED degradation under electrical current*. *Journal of Luminescence*, 2017. **181**: p. 252-260.
25. Samsung. *Why Are Quantum Dot Displays So Good?* 2016; Available from: <https://news.samsung.com/global/why-are-quantum-dot-displays-so-good>.
26. Shirasaki, Y., et al., *Emergence of colloidal quantum-dot light-emitting technologies*. *Nature Photonics*, 2012. **7**(1): p. 13-23.
27. TheEuropeanCommission, *Commission Regulation (EU) 2016/217 of 16 February 2016 amending Annex XVII to Regulation (EC) No 1907/2016 of the European Parliament and of the Council concerning the Registration, Evaluation, Authorisation and Restriction of Chemicals (REACH) as regards cadmium*. *Official Journal of the European Union*, 2016. **L 40/5**.
28. Beloglazova, N.V., et al., *Fluorescently labelled multiplex lateral flow immunoassay based on cadmium-free quantum dots*. *Methods*, 2017. **116**: p. 141-148.
29. Nanite, *Band filling diagram*. 2013: WikiCommons, Public Domain.
30. Vitz, E., et al., *Molecular-orbital energies corresponding to delocalization of valence electrons over increasing numbers of Li atoms. A 1-mg sample of Li would contain nearly 1020 atoms. The corresponding orbital energies are so closely spaced that they constitute essentially continuous bands*. 2017.
31. Neamen, D.A., *Semiconductor Physics and Devices*. 4th ed. 2012: McGraw Hill.
32. esorolla. *Free particle in spherical box*. 2009; Available from: <https://www.physicsforums.com/threads/free-particle-in-spherical-box.329040/>.
33. Brus, L.E., *Electron–electron and electron-hole interactions in small semiconductor crystallites: The size dependence of the lowest excited electronic state*. *The Journal of Chemical Physics*, 1984. **80**(9): p. 4403-4409.
34. Trwoga, P.F., A.J. Kenyon, and C.W. Pitt, *Modeling the contribution of quantum confinement to luminescence from silicon nanoclusters* *Journal of Applied Physics*, 1998. **83**(7): p. 3789-3794.
35. SigmaAldrich, *Splitting of energy levels in quantum dots due to the quantum confinement effect, semiconductor band gap increases with decrease in size of the nanocrystal*. 2012.
36. Reiss, P., J. Bleuse, and A. Pron, *Highly Luminescent CdSe/ZnSe Core/Shell Nanocrystals of Low Size Dispersion*. *Nano Letters*, 2002. **2**(7): p. 781-784.
37. Srivastava, V., et al., *Understanding and Curing Structural Defects in Colloidal GaAs Nanocrystals*. *Nano Lett*, 2017. **17**(3): p. 2094-2101.
38. Anderson, N.C., et al., *Ligand exchange and the stoichiometry of metal chalcogenide nanocrystals: spectroscopic observation of facile metal-carboxylate displacement and binding*. *J Am Chem Soc*, 2013. **135**(49): p. 18536-48.
39. de Mello Donega, C., *Synthesis and properties of colloidal heteronanocrystals*. *Chem Soc Rev*, 2011. **40**(3): p. 1512-46.
40. BerkeleyLab, *Semiconductors for PECs*. 2010: <http://slideplayer.com/slide/6944607/>.
41. Polte, J., *Fundamental growth principles of colloidal metal nanoparticles – a new perspective*. *CrystEngComm*, 2015. **17**(36): p. 6809-6830.

42. Koh, S., et al., *Zinc–Phosphorus Complex Working as an Atomic Valve for Colloidal Growth of Monodisperse Indium Phosphide Quantum Dots*. *Chemistry of Materials*, 2017. **29**(15): p. 6346-6355.
43. Schubert, E.F., *Fig. 7.12. Illustration of two crystals with mismatched lattice constant resulting in dislocations at or near the interface between the two semiconductors*. . <https://www.ecse.rpi.edu/~schubert/Light-Emitting-Diodes-dot-org/chap07/chap07.htm>.
44. Palmer, D.W. *PROPERTIES OF THE II-VI COMPOUND SEMICONDUCTORS*. 2008; Available from: <http://www.semiconductors.co.uk/propiiivi5410.htm>.
45. NSM-IoffeRussia. *InP - Indium Phosphide*. Available from: <http://www.ioffe.ru/SVA/NSM/Semicond/InP/index.html>.
46. Madelung, O., *Semiconductors: Data Handbook*. 3rd ed. 2004: Springer.
47. Nakamura, S., *Light emission moves into the blue*. *Physics World*, 1998. **11**(2): p. 31-35.
48. Stringfellow, G.B. and M. George Craford, *High Brightness Light Emitting Diodes*. Vol. 48. 1997, *Semiconductors and Semimetals*: Academic press.
49. Charifi, Z., et al., *Structural and electronic properties of the wide-gap Zn_{1-x}Mg_xS, Zn_{1-x}Mg_xSe and Zn_{1-x}Mg_xTe ternary alloys*. *Journal of Physics: Condensed Matter*, 2005. **17**(44): p. 7077-7088.
50. Pietra, F., et al., *Ga for Zn Cation Exchange Allows for Highly Luminescent and Photostable InZnP-Based Quantum Dots*. *Chemistry of Materials*, 2017. **29**(12): p. 5192-5199.
51. Ramasamy, P., et al., *Tunable, Bright, and Narrow-Band Luminescence from Colloidal Indium Phosphide Quantum Dots*. *Chemistry of Materials*, 2017. **29**(16): p. 6893-6899.
52. Li, L.S., et al., *High Quality ZnSe and ZnS Nanocrystals Formed by Activating Zinc Carboxylate Precursors*. *Nano Letters*, 2004. **4**(11): p. 2261-2264.
53. Boldt, K., et al., *Electronic Structure Engineering in ZnSe/CdS Type-II Nanoparticles by Interface Alloying*. *The Journal of Physical Chemistry C*, 2014. **118**(24): p. 13276-13284.
54. *Perspective on synthesis, device structures, and printing processes for quantum dot displays* *Optical Materials Express*. **2**(5): p. 594-628.
55. Pietra, F., et al., *Tuning the Lattice Parameter of In_xZn_yP for Highly Luminescent Lattice-Matched Core/Shell Quantum Dots*. *ACS Nano*, 2016. **10**(4): p. 4754-4762.
56. Boldt, K., et al., *Synthesis of Highly Luminescent and Photo-Stable, Graded Shell CdSe/Cd_xZn_{1-x}S Nanoparticles by In Situ Alloying*. *Chemistry of Materials*, 2013. **25**(23): p. 4731-4738.
57. Morrison, P.J., *Synthesis and Characterization of PbS Quantum Sheets Through Lame*, in *PhD thesis, Department of Arts & Sciences, Department of Chemistry*. 2014, Washington University St. Louis.

Appendix

A.1. Derivation for the approximation of a particle in a one dimensional box with infinite potential wells, using the time-independent Schrödinger equation

$$\hat{H} \psi(x) = E \psi(x)$$

$$-\frac{\hbar^2}{2m} \frac{\partial^2 \psi(x)}{\partial x^2} + V(x) \psi(x) = E \psi(x)$$

$$V(x) = 0$$

$$\frac{\partial^2 \psi(x)}{\partial x^2} = -\frac{2mE}{\hbar^2} \psi(x)$$

$$\psi(x) = A \cos(kx) + B \sin(kx) \quad \left(k = \sqrt{\frac{2mE}{\hbar^2}} \right)$$

$$\text{Boundary conditions: } \psi(x=0) = \psi(x=a) = 0$$

$$\psi(x=0) = 0 = A \cos(0) + B \sin(0) = A \rightarrow A = 0$$

$$\psi(x=a) = 0 = B \sin(ka) \rightarrow ka = \sin(0)^{-1} = n\pi$$

$$k_n = \frac{n\pi}{a}$$

$$k^2 \rightarrow k_n^2 = \frac{2mE_n}{\hbar^2} = \left(\frac{n\pi}{a} \right)^2$$

$$E = E_n = \frac{\hbar^2 n^2 \pi^2}{2ma^2} = \frac{h^2 n^2}{8ma^2}$$

A.2. Derivation for the approximation of a particle in a three dimensional box with infinite potential wells, using the time-independent Schrödinger equation

$$\hat{H} \psi(x, y, z) = E \psi(x, y, z)$$

$$\left[-\frac{\hbar^2}{2m} \left(\frac{\partial^2}{\partial x^2} + \frac{\partial^2}{\partial y^2} + \frac{\partial^2}{\partial z^2} \right) + V(x, y, z) \right] \psi(x, y, z) = E \psi(x, y, z)$$

$$V(x, y, z) = \begin{cases} 0 & \text{for } 0 < x < a; \quad 0 < y < b; \quad 0 < z < c \\ \infty & \text{for } x < 0 \text{ and } x > a \\ \infty & \text{for } y < 0 \text{ and } y > b \\ \infty & \text{for } z < 0 \text{ and } z > c \end{cases}$$

$$E_{n_x} = \frac{\hbar^2 n_x^2 \pi^2}{2ma^2}$$

$$E_{n_y} = \frac{\hbar^2 n_y^2 \pi^2}{2mb^2}$$

$$E_{n_z} = \frac{\hbar^2 n_z^2 \pi^2}{2mc^2}$$

$$E_n = E_{n_x} + E_{n_y} + E_{n_z}$$

A.3. Derivation for the change in free energy for the formation of clusters from monomers

$$\Delta G = G_z - \mu_{SS}$$

$$G_z = z\mu_b + \gamma\beta z^{2/3}$$

$$= -z(\mu_{SS} - \mu_b) + \gamma\beta z^{2/3}$$

$$\sigma = \frac{\mu_{SS} - \mu_b}{kT}$$

$$= -zkT\sigma + \gamma\beta z^{2/3}$$

$$A = \beta z^{2/3} = 4\pi r^2$$

$$= -zkT\sigma + \gamma A$$

$$z = \frac{4\pi r^3}{3V_m}$$

$$\Delta G(r) = \frac{-4\pi r^3 kT\sigma}{3V_m} + 4\pi r^2 \gamma$$

A.4. ZnMgSe synthesis with metal stearates and TOP-Se

The first synthesis method tried is based on a protocol mentioned in a PhD thesis from P.J. Morrison, Washington University St. Louis. [57] This synthesis method, developed for the synthesis of pure ZnSe nanoparticles, uses the same precursors as used in the synthesis for the shell of section 5.2. By (partially) substituting zinc stearate for magnesium stearate, as was also done for the shell synthesis in section 5.3., it was tried to synthesize ZnMgSe and MgSe.

The reaction mixture was a clear liquid with a clearly visible blueish white fluorescence as shown in figure FA.1a. The absorption spectra from this synthesis, shown in figure FA.1b., clearly have peaks at 286 nm and 288 nm for the MgSe and the ZnMgSe respectively. Furthermore, the ZnMgSe has a second peak around 340 nm. To prove that these absorption peaks come from formed nanoparticles, TEM and electron diffraction (ED) experiments needed to be performed.

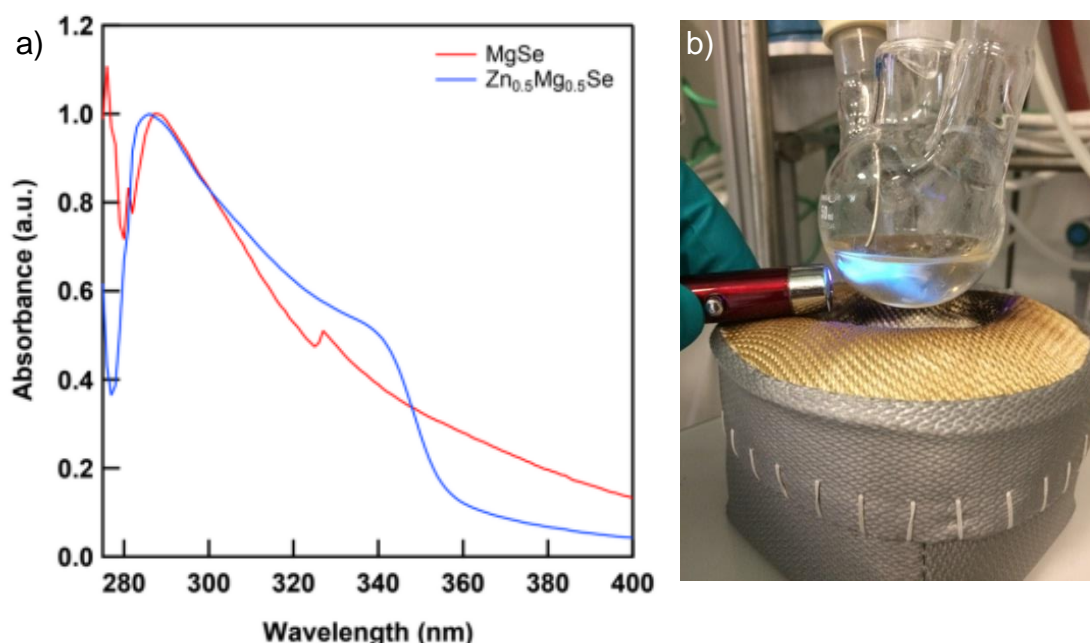


Figure FA.1. Absorption spectra of the adapted synthesis for ZnSe by P.J. Morrison [57], to synthesize MgSe and ZnMgSe. (a) The MgSe synthesis in TOPO, cooled down after a reaction time of 60 minutes shows bright blue emission (b).

Because TOPO, a solid at room temperature, was used for the experiment the nanoparticles formed were difficult to separate from the solvent. Therefore, the TOPO was replaced by ODE. TEM experiments did not show any proof of formed nanoparticles.

To ensure that the metal:Se ratio (4.5:1) was not interfering the results, a control test was set up, to study the effects of an increased metal:Se ratio (2:1) in the reaction mixture. Furthermore, a ZnS shell was grown around the particles, to protect the (Zn)MgSe from oxidation and hydrolysis. Just as for the previous syntheses, a significant difference in color can be observed between the fluorescence from the MgSe/ZnS (figure FA.2a.) and the ZnMgSe/ZnS (figure FA.2b.), indicating that particles with a different band energy have formed. Absorption measurements did not show a clear signal however. TEM imaging also did not show any nanoparticle formation. Therefore, another method was tried to synthesize ZnMgSe nanoparticles.

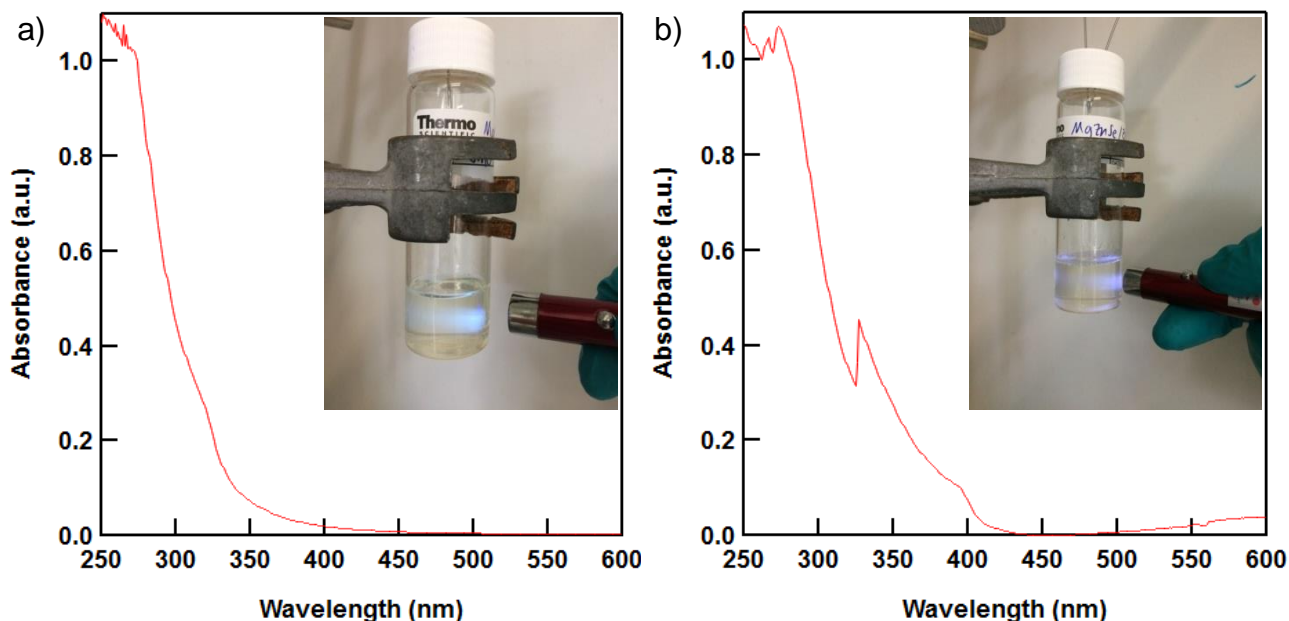


Figure FA.2. MgSe/ZnS (a) and ZnMgSe/ZnS (b) syntheses in ODE, cooled down after a reaction time of 60 minutes. The absorption spectra do not show a small but not clear signal for the formation of nanoparticles.

A.5. Gallium cation exchange on cores

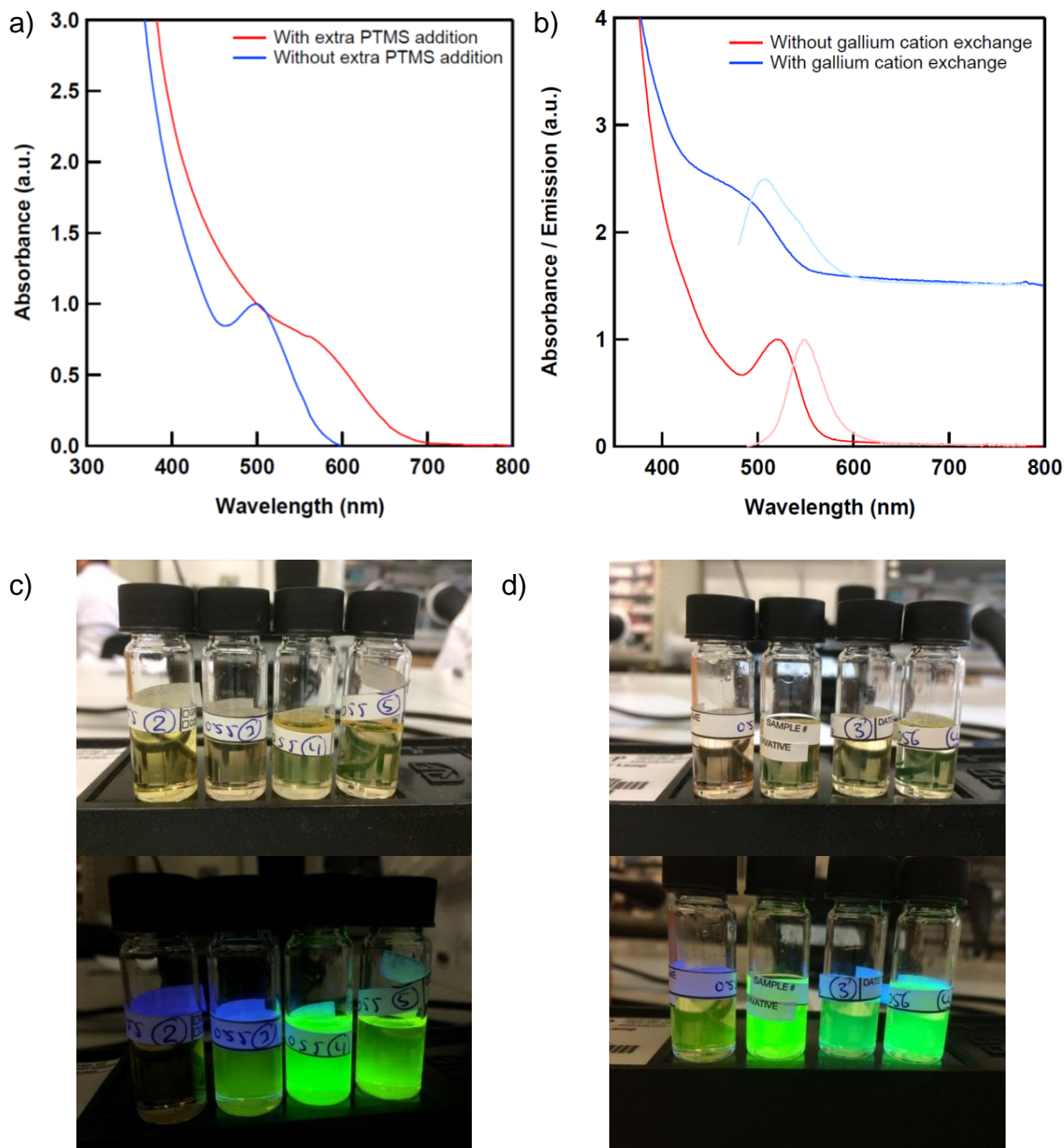
From previously mentioned research [50] it is known that a gallium for zinc cation exchange increases the PLQY of quantum dots, produced by the hot injection method, significantly. The procedure in these articles sometimes includes an extra addition of PTMS to the cores after the gallium cation exchange, to form a GaP shell around the core quantum dot. To test whether this has a positive or negative influence on the properties of the quantum dots, an experiment was performed.

From the absorption data in figure FA.3a., it can be seen that the size distribution for the synthesis with the extra PTMS addition significantly broadens directly after the PTMS addition, compared to the one without extra PTMS addition. Therefore, the extra PTMS addition step was not included in future syntheses protocols.

To furthermore test if the gallium cation exchange also works for the heating up method, an experiment was performed to compare InZnP/ZnMgSe/ZnS core shell shell quantum dots with and without gallium exchange on the cores.

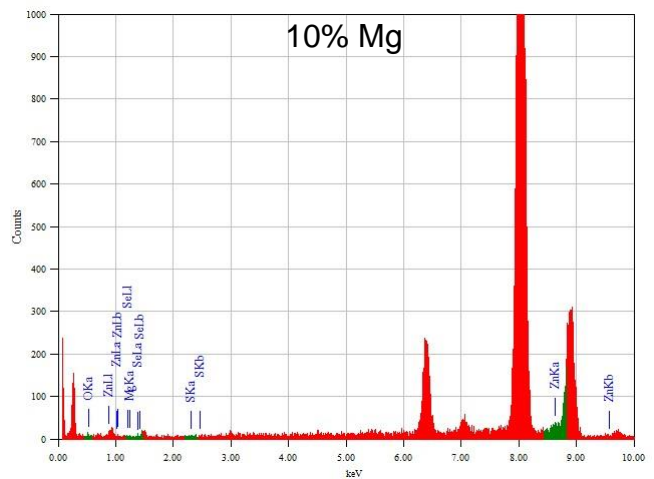
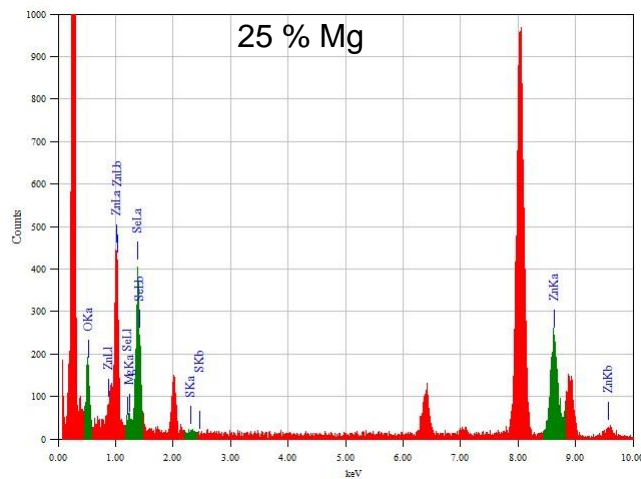
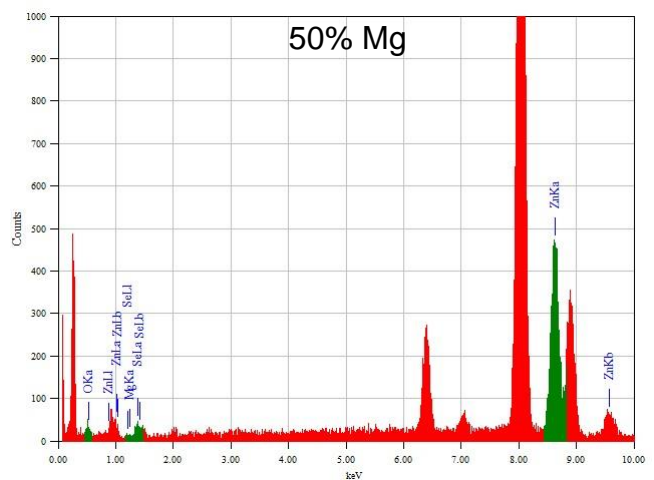
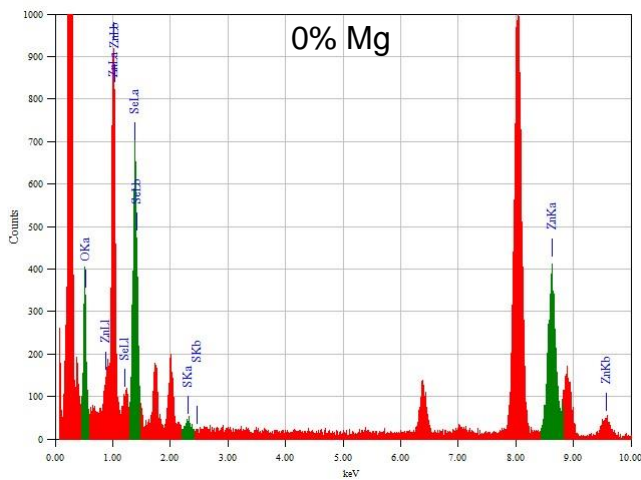
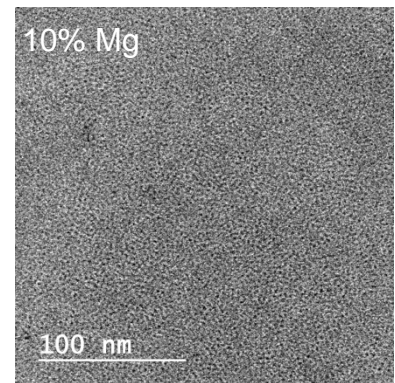
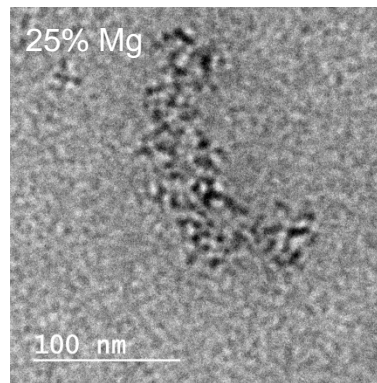
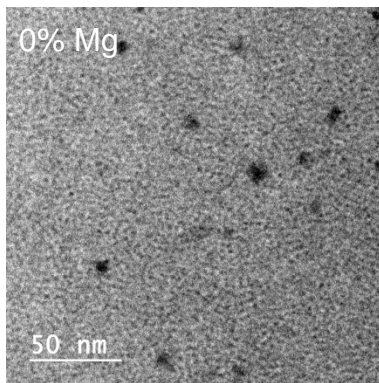
The results, shown in figure FA.3b., indicate that with the gallium exchange, the absorption blue-shifts by the gallium cation exchange. The emission does not seem to be influenced much by eye (figures FA.3c,d.). The absorption is somewhat broadened compared to the quantum dots without gallium cation exchange.

After a ZnS shell is grown around both quantum dots, the absorption of the quantum dots which had a gallium cation exchange is significantly broadened, and at the same time, the emission decreased visibly.



FA.3. InZnP quantum dots after gallium cation exchange, with and without the addition of PTMS to form a GaP shell (a). The emission significantly blue-shifts after a gallium exchange (b) which cannot clearly be seen from the samples with (c) and without gallium exchange (d).

A.6. TEM and EDX data section 7.3.



Magnesium fraction reactants	Zinc fraction from EDX	magnesium fraction from EDX	Selenium fraction from EDX	Sulfur fraction from EDX	Oxygen fraction from EDX
0%	31	0	67	5	7
25%	34	3.5	37.5	0.5	24.5
50%	91	0	3	Not measured	6

Jence Mulder

Delft University of Technology
Faculty of applied sciences
Department of Chemical Engineering

March 8th, 2018